

FINAL PUBLISHABLE JRP REPORT

JRP-Contract number	SIB51	
JRP short name	GraphOhm	
JRP full title	Quantum resistance metrology based on graphene	
Version numbers of latest contracted Annex Ia and Annex Ib against which the assessment will be made	Annex Ia:	V1.0
	Annex Ib:	V1.0
Period covered (dates)	From 1 June 2013	To 31 May 2016
JRP-Coordinator		
Name, title, organisation	Dr Franz Josef Ahlers, PTB	
Tel:	+49 531 592 2600	
Email:	franz.ahlers@ptb.de	
JRP website address	http://www.ptb.de/emrp/graphohm.html	
Other JRP-Partners		
Short name, country	CMI, Czech Republic	
	LNE, France	
	METAS, Switzerland	
	VTT, Finland	
	NPL, United Kingdom	
	SMU, Slovakia	
	RISE, Sweden	
	KRISS, Republic of Korea	
REG1-Researcher (associated Home Organisation)	Dr Sergey Kubatkin (Chalmers, Sweden)	Start date: 1 June 2013 Duration: 36
REG2-Researcher (associated Home Organisation)	Dr Rositsa Yakimova (LiU, Sweden)	Start date: 1 June 2013 Duration: 36
REG3-Researcher (associated Home Organisation)	Dr Andrey Turchanin (UBI, Germany)	Start date: 1 November 2013 Duration: 26

Report Status: PU Public

TABLE OF CONTENTS

1	Executive Summary	3
2	Project context, rationale and objectives	4
2.1	Context.....	4
2.2	Objectives.....	5
3	Research results.....	6
3.1	Development and advancement of graphene and graphene device fabrication	6
3.2	Development of better characterisation methods	14
3.3	Exploration of the limits of graphene in precision resistance metrology	20
3.4	Assessment of the potential of graphene for impedance metrology	29
3.5	Development of bespoke instrumentation for a simplified use of graphene	34
3.6	Summary of the key results and conclusions	36
4	Actual and potential impact.....	37
4.1	Metrology achievements.....	37
4.2	Examples of early impact.....	38
4.3	Dissemination activities.....	38
4.4	Potential impact.....	39
4.5	Projected JRP impact on EC Directives, and other relevant standards	39
5	Website address and contact details.....	40
6	List of publications	41

1 Executive Summary

Introduction

The units of electricity play a key role in industrial, scientific and technological applications since the measurement of nearly all other quantities relies on them at some point. Electrical resistance is traced to the quantum standard using the quantum Hall effect (QHE, a quantum electronic effect that allows accurate realisation of Planck's constant and elementary charge). This project developed a QHE system using accurate and simple to use standards of electrical resistance based on graphene. Graphene, the two-dimensional crystal of carbon, has many extraordinary properties and characteristics which surpass those of other materials. This project paves the way to a robust, simpler to operate and cheaper, yet precise system for electrical measurements. This will benefit all NMIs, measurement services in Europe, and all industries relying on their service.

The Problem

While quantum electrical voltage standards are widespread and easily transported, primary quantum resistance standards are only available at national measurement institutes (NMIs) and the resulting calibrations lose precision at every link of their long chain, which leads to a loss of time and money due to periodic recalibrations of secondary standards. Up until now the equipment needed for exploiting the QHE is very specialised and expensive and requires highly experienced staff.

A QHE system which is simpler, transportable, and provides the primary reference closer to the end user will reduce the cost and inconvenience of traditional calibration chains, constituting a real breakthrough for European and worldwide metrology.

The Solution

Graphene exhibits the QHE at lower magnetic fields and closer to room temperature than any other material, offering an opportunity to create a QHE system using graphene and widely available laboratory equipment, such as simple cryo-coolers and liquid helium dewars. The material could therefore help to create simple and portable 'bench-top' systems which could be deployed more widely and easily than current resistance standards, - into smaller NMIs, into industry, or allowing a dedicated QHE reference at the point of use.

This project underpins this opportunity by addressing advanced fabrication methods for graphene materials, methods for its reliable characterisation, the testing of the precision limits with respect to temperature, magnetic field and measurement current, as well as the development of dedicated simplified measurement equipment, in order to investigate and produce a graphene QHE resistance standard and simplify the resistance traceability chain.

Impact

This project used materials science and improved measurement precision to build stable graphene devices that can operate in relaxed conditions of higher temperature and lower magnetic field, and can be used as quantum resistance standards for the electricity community. The results have considerably advanced the ability to utilise the quantum based representation of resistance and impedance measurement units.

As project collaborators, the acknowledgement and involvement of the Bureau International des Poids et Mesures, BIPM, was valuable in ensuring maximum impact in the worldwide measurement system.

This acknowledgement is reflected in the [March 2015 News article](#) of the Consultative Committee for Electricity and Magnetism, CCEM, which states that "*Significant progress on the quantum Hall effect with graphene samples ... will lead to simpler and lower cost quantum resistance standards, and in consequence to their wider use.*"

In addition, the collaboration between BIPM and the project is highlighted in a [September 2015 News article of BIPM](#) which says that "*In the ... GraphOhm EURAMET project, samples developed ... proved suitable for calibration ... (BIPM) envisage(s) being able to implement a much simplified transportable system ... The collaboration ... also involved the investigation of a new generation of (instrumentation) ... that could ... accompany the new graphene reference.*"

The outputs of the project have already been taken up by several industrial companies who are developing systems that utilise the benefits of the graphene technology developed during the project, including:

- UK based Oxford Instruments plc, collaborating with NPL, has produced a closed cycle cooler system adapted for graphene QHE measurements which is now available.
- Swedish based company GraphenSIC, linked to Linköping University, has produced a compact low-field magnet insert for Helium dewars, including a graphene QHE device, which is now available.
- Canada based company Measurement International, cooperating with the project consortium announced production and marketing of a dedicated graphene QHE resistance standard system.

The ability to measure quantum electrical resistance and impedance precisely by the end user, with a reduced length calibration chain, will save money and time for end users.

Parts of such characterisation systems, like dedicated cryo-coolers are available already. Knowledge transfer programmes in national or European funding schemes have the potential to lead to a complete and standalone commercial system within the next five years.

2 Project context, rationale and objectives

2.1 Context

Electrical resistance, the ratio of applied voltage and current in an electrical circuit, is one of the most important of all measurement quantities, from a fundamental as well as from a practical point of view.

The *fundamental reason* for its importance is its role in the forthcoming revision of the International System of Units, SI, scheduled for 2019. In the revised SI, a resistance R will be traced to a combination of two fundamental constants, Planck's constant h , and elementary charge e . When resistance is combined with electrical voltage U , derived from another combination of the same constants, also the unit of mass, the kilogram, can be traced to h by exploiting the relation for electrical power, $P = U^2 / R$, in an electromechanical balance, the so-called Kibble balance. The thus established connection between mechanical and electrical units will be the key cornerstone of the revised SI.

The *practical reason* for the importance of electrical resistance results from the outstanding role which 'electronics' plays in almost all areas of industry, science, and technology. The function of electric circuits is determined by the ratios of voltages and currents, and for developing any kind of electronics it is essential to know the resistance of the electrical components. A *further practical reason* is the strong dependence of resistance on material properties and temperature which is exploited in resistive sensors. Resistance thermometers, for example, are the most widely used type of thermometer, and the determination of many other material properties is often done via a measurement of resistance values.

The unit of temperature, Kelvin, will in future be derived from the value of the Boltzmann constant, k_B . The most promising practical realisation will make use of the Johnson-Nyquist noise of a resistor, whose value has to be known precisely. This once more underpins the importance of the unit of resistance.

The effect which allows the direct tracing of a voltage/current ratio to h and e is the quantised Hall Effect, QHE. After its discovery in 1980 the precision of resistance measurements was nearly immediately boosted by some two orders of magnitude. Only ten years later, in 1990, such a high precision was reached, that by international agreement it was decided to perform all electrical measurements within a sub-system of the SI, called 'conventional electrical units' system. This situation will be resolved by the revision of the SI.

However, the practical use of the QHE always remained restricted to only a few high-level standards institutes, due to demanding QHE operation conditions which required very low temperatures and very high magnetic fields.

While the QHE had boosted the accuracy level of measurements considerably, the restrictions for its practical use needed to be relaxed in order to bring this accuracy improvement closer to the industrial end users. No user of metrological services, and often not even national measurement institutes (NMIs), could take direct advantage from the perfect fundamental constant based standards for the reasons mentioned above. While systems for the unit of voltage can easily be transported and were widespread already, there was a need to achieve the same level of simple dissemination for quantum standards of resistance.

Graphene, a flat regular honeycomb network of carbon atoms, allows observing the QHE at much higher temperature and much lower magnetic field than any material known before. However, after the

demonstration of its basic suitability as a quantum resistance standard, the technology steps to develop a simple to use *quantum resistance system* around it still needed to be made.

To this end several issues had to be addressed. The improvement of the material, of methods for its reliable characterisation, the testing of the precision limits with respect to temperature, magnetic field, and measurement current, as well as the development of dedicated simplified measurement equipment were the main topics addressed in the project.

2.2 Objectives

The outcomes of this project are key components for a simplified primary resistance standard, namely a new type of quantum device, the established technology to produce it, and the prototype measurement setup to make optimal use of it. With these key components industrial collaborators have the chance to transform them into a commercial system. Such a system will eventually allow small country NMIs, dedicated calibration labs, and calibration departments in companies to provide the best possible calibration services for the quantities electrical resistance and capacitance.

Specifically, the following five main objectives were addressed:

- **Advanced fabrication methods for graphene materials and of QHE devices** to fulfil requirements in terms of homogeneity, contact resistance, size. The goal is fabrication of graphene material and devices with optimised parameters, which are stable under typical usage conditions involving repeated cool-down cycles.
- **Develop procedures for precise, quantitative, non-destructive characterisation** of graphene and graphene devices combining structural, chemical and physical methods.
- **Explore and understand the limits of achievable uncertainty** by precision QHE measurements on graphene under less demanding experimental requirements of temperature and magnetic field.
- **Assess the potential of a graphene-based impedance standard** by investigating ac-losses in graphene devices and demonstrate the QHE effect at ac frequencies in graphene.
- **Develop customised cooling and measurement instrumentation** to support the simplified use of a graphene resistance standard. This includes a non-cryogenic measurement bridge with performance similar to that of a cryogenic one.

The advancement of fabrication of graphene as well as of devices based on graphene is an absolute prerequisite for its use in metrology. Metrological requirements often differ strongly from typical requirements in, e.g., electronics industry production cycles. Large dimensions of the active electrical part, an extremely high homogeneity across those dimensions, and the maintenance of these properties during subsequent stages of processing are typical such requirements.

Characterisation methods during all stages of development are needed to control the processes, and they need to be tailored to the special requirements of the material. They should at the same time be simple in application, reliable in their results, and economic to establish and use.

The metrological core of the project was the exploration of the limits (in terms of operating temperature, drive current, and magnetic field) under which precision QHE measurements on graphene can be performed. The clearly set goal at project start was to demonstrate a relative uncertainty below 1 part in 10^8 above 4 K in temperature at a magnetic field below 5 T with current levels in the tens of μA range.

Operating QHE devices at ac-frequencies should also allow them to be used as a quantum standard of impedance, but this had been shown only for GaAs-based devices. In order to assess the potential of graphene for this additional application dimension, the project set out to investigate ac-losses in graphene devices and to demonstrate the ac-QHE effect.

Finally, a simplified standard with potential for knowledge transfer also needs customised instrumentation to simplify its daily use. This specifically includes vital instrumentation for scaling of the singular QHE value of 12.9 k Ω to the full range of resistance values relevant in practice, and which does not require liquid helium for cooling.

3 Research results

3.1 Development and advancement of graphene and graphene device fabrication

The advancement of the fabrication of graphene as well as of devices based on graphene is an absolute prerequisite for its use in metrology. At project launch, several partners dedicated resources to the graphene growth task (LiU and KRISS) and to the graphene device fabrication task (Chalmers, RISE, KRISS, and PTB). Rather early it became obvious that more efforts are highly desirable, for work to be done within the project, as well as for additional development threads with scope beyond the project. Therefore, graphene growth capabilities were also established at VTT (in cooperation with Aalto university), at LNE (in cooperation with CNRS institutes), and at PTB.

3.1.1 Fabrication of epitaxial and CVD graphene films

The methods for the growth of graphene material have been considerably advanced in the project. One of the main challenges during the growth of graphene on silicon carbide (SiC) crystals is the avoidance of bi-layer graphene. Bilayers would render the material unsuitable for precision QHE applications, but they form all too easily along the terrace steps of the host SiC substrate, either as stripes or as non-connected patches. Thanks to the close feedback from new characterisation methods developed in parallel the problem could be solved successfully by carefully improving the complex growth sequence. This sequence is not just relevant for the actual growth step, but even more so for the substrate pre-conditioning phases which have to be passed before the graphene formation temperature of around 1600 – 1800 °C is reached.

Growth of SiC-graphene on the wafer scale was also achieved, which opens more opportunities, e.g. for the fabrication of arrays of QHE-devices suitable for realising a whole range of resistance values. Further to this, in a collaborating institute a variant of the established SiC-graphene growth was developed, which holds promise to yield graphene of similarly excellent, maybe even better quality. The remaining, but unavoidable issue with SiC-grown graphene, namely its very high density of electrons, could be considerably relaxed by developing a new method where a corona discharge is used to reduce the carrier density by depositing ions in a resist layer covering the graphene film.

Epitaxial graphene at LiU

At LiU work concentrated on optimising the graphene growth regimes, on achieving high mobility and well-controlled and uniform carrier concentration, and on optimising the substrate selection and surface treatment prior to graphene growth with the view to achieve defect- and strain-free uniform graphene monolayers.

The main target was growth of epitaxial graphene on SiC with parameters meeting the requirements for robust quantum hall effect (QHE). In order to obtain large area monolayer (ML) the existing infrastructure was upgraded by designing and building a 4-inch reactor. Along with optimisation of the smaller reactor in terms of crucible and temperature conditions, temperature uniformity over the large crucible and graphene thickness uniformity were studied. The 4-inch graphene growth set-up and a cross section of the new crucible are shown in Fig. 1.

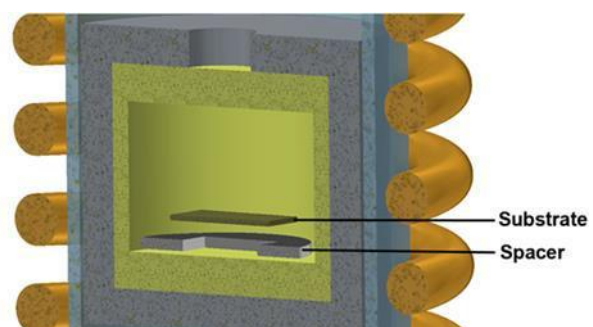
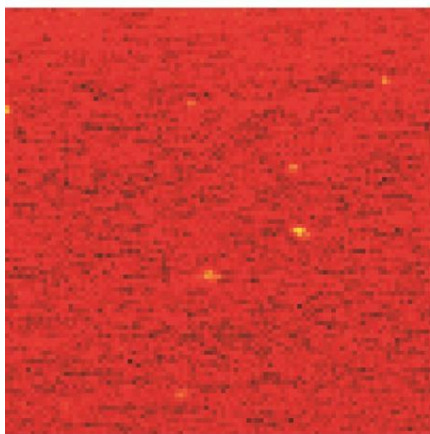


Fig. 1 Epitaxial graphene growth set up (left) and the growth crucible in a cross section

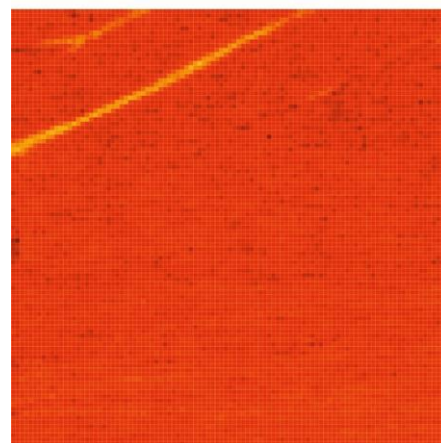
ML graphene with high mobility over a large area is the targeted material for a stable quantum Hall resistance standard development. Not only is the reproducibility of the results crucial for the yield, respectively cost efficiency of the fabrication processes, but also one has to avoid the creation of bilayer graphene patches. LiU has succeeded to suppress the bilayer formation down to 0.1% on 7x7 cm² samples and 1.4% on samples of 20x20 mm² area. The conclusion is that with increasing the substrate area, fine tuning of the growth conditions is required. For this attention should be paid to the kinetics of the buffer layer completion, which can be monitored by ex-situ Raman measurements. By using that LiU has got indications that the first layer of graphene may not be completely detached from the buffer layer which is a reason for the low carrier mobility. Fig. 2 illustrates the improvement of the ML uniformity while sample size is increasing.

G808, Step 300 nm, Map30.0x30.0 μm



1L: 99.804%
2L: .196%

G722-prm1, Step 300 nm, Map30.0x30.0 μm



1L: 98.6%
2L: 1.4%

Fig. 2 Thickness uniformity mapping of epitaxial graphene on SiC: 0.1% bilayer on 7x7 mm² and 1.4% on 20x20 mm². The images are obtained by optical reflectance in a Raman set-up.

Raman spectroscopy has been used for detailed analysis and understanding the role of the buffer layer, which is not a conventional approach. Carrier mobility has been assessed by Van der Pauw measurements on large samples showing mobility numbers up to 3 500 cm²/Vs at room temperature. New contactless measurements were employed as a training activity by other partners. New method for SiC surface preparation by sublimation etching has been proposed (Surface engineering of SiC substrates via sublimation etching, accepted in Surface and Interfaces, 2016). Preferred substrate is 4H-SiC purchased from Cree Ltd, USA.

The achievements related to graphene material perfection in this project have allowed unique advancements in the area of quantum metrology. It was also possible to transfer knowledge to partners and to contribute to the spin off company Graphensic established in 2011.

Epitaxial graphene at PTB

During the project, PTB has also set up a graphene growth facility for growth on 10x10 mm² SiC chips. PTB followed the proven designs originally developed by Th. Seyller (University of Chemnitz) and R. Yakimova (LiU). Rapid progress was made, and now excellent graphene can also be produced at PTB. Most noteworthy is a new growth method developed at PTB which enables the growth of virtually bilayer-free graphene. Bilayers on top of the QHE-active monolayers would be extremely detrimental to the achievable precision since they can act as electric shorts between opposing edges of the Hall device.

At the heart of the new method (patent application submitted) is the addition of excess carbon made available by thermal decomposition of a dilute polymer, which is applied prior to the growth process. Fig. 3 shows a map of colour coded Raman line widths which proves the monolayer quality of the graphene grown with the new method.

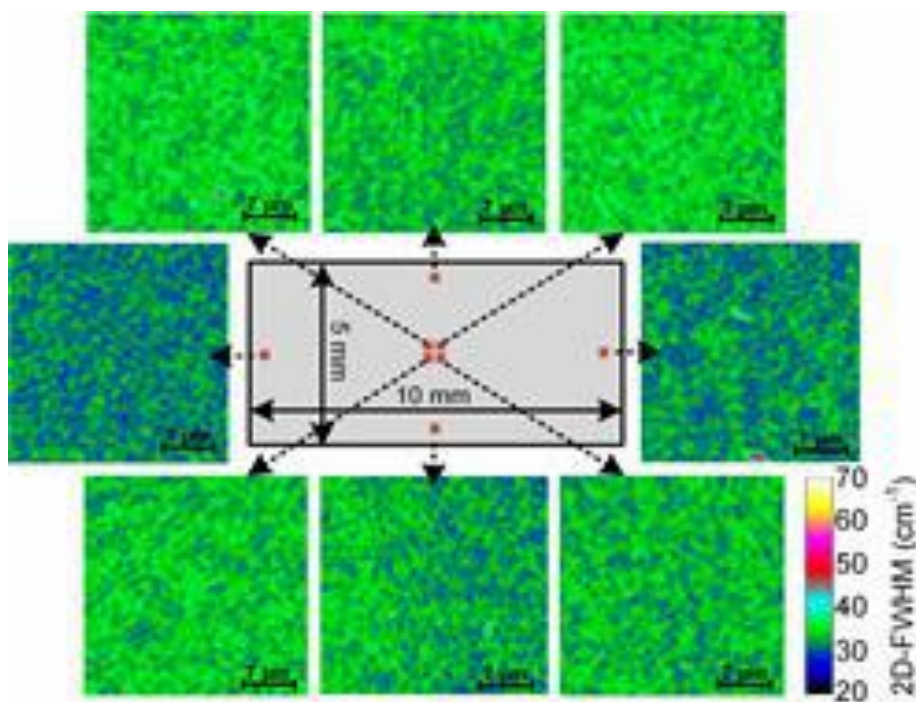


Fig. 3 Raman maps taken at 8 different positions from a 5x10 mm² SiC chip after graphene growth. In the false colour plot the colours represent the width of the characteristic Raman 2D line as an indicator of the layer count of the fabricated graphene. Monolayer graphene is represented by green-blue regions, and the (only sparsely occurring) red regions indicate bilayer graphene. Only spots occur, but no patches.

Epitaxial graphene at LNE

LNE collaborated with the *Centre de Recherches sur l'hétéro-épitaxie et ses applications du Centre National de la Recherche Scientifique (CRHEA-CNRS)*, where graphene was also grown on SiC, but with another variant of the standard growth method: Graphene was grown by propane/hydrogen CVD on the Si-face of a semi-insulating 0.16° off-axis 6H-SiC substrate. Angle-resolved photoemission spectroscopy (ARPES) and low-energy electron microscopy (LEEM) revealed that a graphene monolayer covers almost the whole SiC substrate (Fig. 4-Left), but that about 10-15 % is covered by a second graphene layer (Fig. 4-Right). Low electron-energy diffraction (LEED) showed the existence of a $6R\sqrt{3} \times 6R\sqrt{3} - R30^\circ$ reconstructed carbon-rich interface (buffer layer) between the substrate and the graphene monolayer. Large Hall bars of 100 x 420 μm² size with eight terminals were patterned at the *Laboratoire de Photonique et Nanostructures (LPN-CNRS)* using electron beam lithography with poly-methylmethacrylate (PMMA) resist and oxygen reactive ion etching (RIE). Ohmic contacts to the graphene layer were formed by depositing a Pd/Au (60 nm/20 nm) bilayer in an electron-beam deposition system, using an ultrathin Ti layer for adhesion. Thicker Ti/Au (20 nm/200 nm) bonding pads were formed in a subsequent step. Samples were covered for protection by 300 nm of poly(methylmethacrylate-co-methacrylate acid) copolymer (MMA (8.5) MAAEL10 from Microchem) and 300 nm of poly(methylstyrene-co-chloromethylacrylate) (ZEP520A from Zeon Chemicals) resist. The ZEP520A resist is known to reduce the electron density under ultraviolet illumination. Nonetheless, no illumination was done in this case. LNE investigated the QHE in two of these samples, as described in section "*Measurements on SiC-CVD graphene*" on page 26.

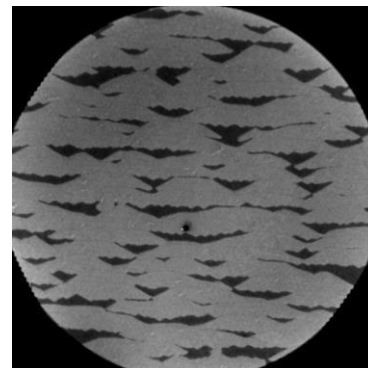
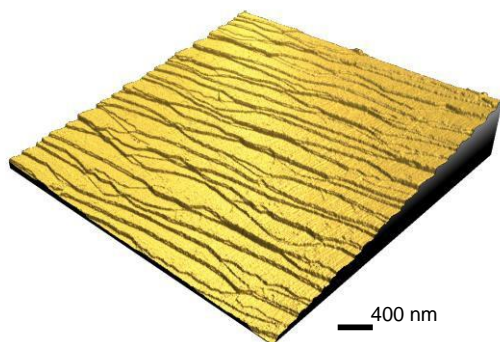


Fig. 4-Left: Atomic force microscopy image of the SiC substrate after graphene growth showing about 300 nm SiC steps. Right: Low electron-energy microscopy image showing small bilayer patches covering about 10% of the surface. The image width is 10 μm .

CVD graphene

Chemical vapour deposition (CVD) has been employed as an important method for the preparation and production of large-area graphene. CVD on transition metal substrates (Cu, Ni, Pt) has become a promising approach due to a controllable growth process, which is inexpensive and able to produce large-area graphene.

However, the method requires a transfer of the graphene films from the metallic growth template to an insulating substrate, which is usually Si covered by SiO₂. Degradation of the graphene films during transfer is extremely hard to avoid, and the fact that large films mostly consist of mono-crystalline domains with domain boundaries in between prevent their use for precision QHE measurements.

Especially the latter decisive fact was only established definitively during this project by the work of LNE and its collaborators. At project start, the partners had set out to study CVD graphene as an alternative to SiC-graphene. Besides LNE, KRISS was also active in this field. KRISS undertook the challenge to grow graphene on and between two-dimensional layers of hexagonal boron nitride (h-BN), which is, like graphene, a hexagonally coordinated crystal with very favourable properties as a graphene host substrate.

LNE cooperated with the *Institut Néel* (group Vincent Bouchiat) and studied Hall bar devices made by that group, which were based on polycrystalline graphene produced by CVD on copper foils from a hydrogen/methane mixture. Graphene had been transferred onto a Si wafer with 285 nm-thick SiO₂ layer, by etching the underneath Cu, using (NH₄)₂S₂O₈ solution. The Hall bar samples studied, of channel width between 5 μm and 200 μm , were fabricated by optical lithography and oxygen plasma etching and contacted with Ti and Au (5 and 60 nm) electrodes. These measurements are presented in section “Measurements on CVD graphene” on page 26.

KRISS established a CVD growing system and pursued it to advance the quality of graphene films synthesised by the CVD method with various synthesis conditions such as substrate, partial pressure, gas mixture and substrate pre-treatment.

The KRISS growing process for the synthesis of large-area and high-quality graphene films on copper foils is as follows: After electro polishing and annealing of the substrate at a temperature of 1293 K for 40 min, copper foil is heated inside a furnace under H₂ gas pressure of (0.1 ~ 2) sccm up to 1293 K for about 30 min. Graphene is grown on the Cu foil held at a growth temperature of about 1293 K under controlled CH₄ (0.5 sccm) and H₂ (8 sccm) gas flow for a controlled time of 15 min. The growth process of graphene islands on a Cu foil was studied with SEM and Raman spectroscopy. Various shapes of graphene domains caused by growth conditions were observed using scanning electron microscopy (SEM) images. Once the nucleation of graphene starts, the number of nucleation sites increase with different size of graphene islands. The islands start to diffuse if the temperature is high enough and coalesce to form a large cluster via island diffusion. However, the edge diffusion is limited because of rebonding during the growth process.

In Raman spectra of CVD graphene transferred onto Si/SiO₂, the D peak around 1345 cm⁻¹, indicative of

defects, is not observable. G and 2D peaks of graphene on SiO₂ are located at 1584 and 2684 cm⁻¹. The intensity ratio between G and 2D peaks is smaller than 0.4, which implies growth of monolayer graphene.

CVD graphene on CVD h-BN

The electrical properties of graphene are strongly influenced by charged impurities of an oxide substrate such as SiO₂. h-BN as a substrate is considered the most suitable one to eliminate such problematic surface effects. It is a III-IV compound with a structure very similar to graphene, and its honeycomb structure is composed of alternating boron and nitrogen atoms. h-BN has a large band gap and does not have dangling bonds. In addition, it is comparatively inert and features a low density of charged impurities.

At KRISS, the growth of large-area monolayer h-BN was performed on 25 μm-thick Cu foil using CVD under low pressure (33 hPa). The Cu foil was electro polished to remove impurities and obtain a flat Cu foil. To remove the oxide layer of the Cu foil, it was annealed at 1263 K for 30 min with H₂ gas at a rate of (0.2 ~ 1 sccm). Ammonia borane was thermally decomposed to hydrogen, monomeric aminoborane, and borazine at temperatures from 353 K to 393 K. After thermal treatment, h-BN was synthesised with borazine gas and hydrogen at 1270 K for 30 min. After growing h-BN films on Cu foil, the films were transferred onto SiO₂ to analyse their properties. Next, CVD graphene was transferred onto the h-BN film using the conventional transfer method. After having made contact electrodes, an additional h-BN layer was transferred onto the graphene/h-BN film, in order to finally obtain a sandwiched h-BN/graphene/h-BN film.

The growth of a CVD h-BN film on Cu foil was confirmed using AFM and SEM. A typical grain size of h-BN is about 5 ~ 10 μm. Triangle shaped h-BN islands were observed in the initial growth process. Once the h-BN islands start to nucleate, they increase in size and density. The islands coalesce to eventually form a complete layer. In the Raman spectra of CVD h-BN on silicon, the h-BN peak was observed at 1369 cm⁻¹, clearly distinct from the graphene G peak at 1583 cm⁻¹. It is, however, hardly distinguishable from the defect-indicating graphene D peak at 1345 cm⁻¹. The Raman G and 2D peaks of CVD graphene depend on the substrates SiO₂ and h-BN. On SiO₂ they are located at 1584 and 2684 cm⁻¹, respectively, whereas on h-BN they are at 1581 and 2688 cm⁻¹. In the case of graphene sandwiched between CVD h-BN films, the G and 2D peak positions are nearly the same as those of graphene on h-BN. The red-shift of the G-peak of graphene on h-BN with respect to that on SiO₂ can be attributed to a reduced doping effect. This reduced doping effect was confirmed by the increased width of the G-peak. The G-peak position of the sandwiched graphene, h-BN/graphene/h-BN, observed at 1581 cm⁻¹ is similar as the peak of the graphene on h-BN. The quality of graphene depends on substrates. The intensity ratio between 2D and G, the G-and 2D-peak positions, and the width of the 2D peak show a large scatter for graphene on SiO₂ and a small scatter for the sandwiched graphene.

Electrical transport properties of the CVD graphene were characterised using Hall devices. They were fabricated by e-beam lithography and O₂ plasma etching. After patterning an isolated graphene channel by etching, the electrode pad for the Hall bar was patterned by E-beam lithography, followed by deposition of Ti (3 nm)/Au (40 nm) in an E-beam evaporator.

Using a probe station at room temperature to check the device, a Dirac voltage of about 1.5 V was measured. The resistance was typically of the order of 100 Ω/μm. At about 2 K, the Dirac voltage was about 13 V, and the Drude mobility was strongly dependent on the device fabrication process with values between 5000 cm²/Vs and 20 000 cm²/Vs. The increase of the charge neutrality voltage at low temperature indicates that doping of graphene has occurred during the device fabrication process.

Even though a higher carrier mobility was observed in the graphene/h-BN and the sandwiched films, the quality of the graphene transferred onto CVD grown h-BN is not as good as the directly grown CVD graphene on Cu foil. Although the CVD-grown h-BN should in principle provide an ideal substrate for graphene, a direct growth of high-quality CVD graphene on CVD h-BN is necessary to avoid the formation of residues between the graphene and the h-BN layer resulting from a transfer process.

Patterned graphene growth

In many applications, an intricate patterning process for fabricating the micro (or nano) structured graphene is essential. Generally, common patterning methods require several steps such as lithographic techniques and often aggressive etching, resulting in damage and poor quality of graphene. To avoid this, KRISS developed a facile route for patterned growth of a graphene/amorphous carbon lateral junction in a single-step process.

In the patterned growth of graphene, graphene/amorphous carbon (G/a-C) heterostructures are grown in a single step from a solid source of polystyrene (PS) via a selective photo-crosslinking process. When the PS film is exposed directly to UV, this region is modified to crosslinked PS (CPS). CPS suffers only minimal decomposition into hydrocarbon vapours due to its high thermal stability, and so it simply converts into a-C at high temperatures, while non-exposed PS regions convert to graphene. In this way CVD growth of the G/a-C heterostructure using crosslinking-driven chemical patterning of a solid carbon source of PS is obtained.

After transferring G/a-C heterostructures onto a SiO₂/Si substrate, two regions (graphene and a-C) are clearly distinguishable in optical microscope and SEM images. To characterise the quality and uniformity of a G/a-C heterostructure on a SiO₂/Si substrate, Raman spectroscopy at 532 nm is used. The Raman spectrum of graphene in G/a-C heterostructures is almost the same as that of pristine graphene. The relative intensity of the defect indicating D-peak to the G-peak is as small as 0.05. Raman maps based on the frequency of G and 2D peaks illustrate that the G/a-C heterostructures are uniform throughout the entire area.

The electrical properties of the G/a-C heterostructures were studied by fabricating field-effect transistor (FETs) devices. The electron/hole mobility was 3500 cm²V⁻¹s⁻¹. The quantum Hall effect of graphene was demonstrated by measuring the resistance versus gate bias at a temperature of 4 K and a high magnetic field of 15 T. Unlike conventional fabrication of graphene Hall bars on SiO₂/Si substrate with lithographic techniques, the electrodes were directly fabricated on the stripe-typed alternating G/a-C heterostructure film without plasma etching process to isolate the device channel area. The half-integer QHE with plateaus at filling factors $\nu=2$ and 4 was observed. The sequence of plateaus for both electron and hole regimes shows the existence of edge states in the structure, indicating that the intrinsic property of graphene is well maintained in the G/a-C heterostructure-based Hall device. However, a slight deviation from the correctly quantised values was observed in both regimes. Furthermore, weak localisation and activation energy with variation in temperature were observed.

The ability to directly synthesise patterned graphene from a polymer pattern opens up new possibilities for the preparation of versatile heterostructures. Flexible devices fabricated from the G/a-C heterostructure show high mobility and excellent mechanical stability against bending. Measurement of the quantum Hall effect in G/a-C lateral heterostructures shows the reliable quality of graphene and well-defined G/a-C interface. However, improvements of the graphene quality are needed for a metrological application.

3.1.2 Hall bar device micro-fabrication

The processing of epitaxial graphene on silicon carbide (SiC) into Hall bars suitable for metrological applications has been considerably advanced. Chalmers has developed an express analysis method of the graphene quality to evaluate the amount and the morphology of bilayer patches, a control method of carrier density in graphene towards the low densities, and fabrication protocols allowing medium scale integration of up to 100 hall bars on the wafer. In addition, they have transferred know-how of developed expertise to other participants of the consortium. In detail, the following achievements were made:

- It was demonstrated that inspection with an optical microscope allows surprisingly simple and accurate identification of single and multilayer graphene domains in epitaxial graphene on silicon carbide (SiC/G). This is informative about nanoscopic details of the SiC topography, making it ideal for rapid and non-invasive quality control of as-grown SiC/G. Fig. 5 (Left) shows a transmission optical image of hall bar C4 on wafer G442, Hall bar width is 50 μm . This is selected as one suitable candidate for quantum hall effect due to geometry and low content of bilayer patches present within the device. (Bilayers appear as darker regions). Right – fully developed quantum Hall state measured for this device at 2K.
- It was demonstrated that reversible carrier density control across the Dirac point in epitaxial graphene on SiC (SiC/G) is possible via high electrostatic potential gating with ions produced by a corona discharge. The method is attractive for applications where graphene with a fixed carrier density is needed, such as quantum metrology, and more generally as a simple method of gating 2DEGs formed at semiconductor interfaces and in topological insulators.

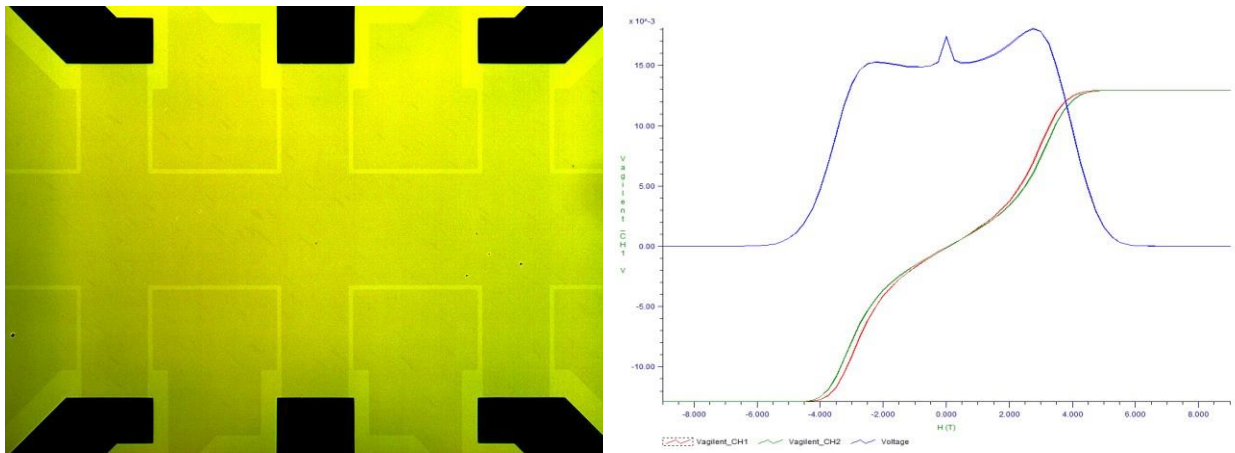


Fig. 5 Left – Transmission optical image of fabricated hall bar C4 on wafer G442. Hall bar width is 50 μm . Right – fully developed quantum Hall state measured for this device at 2K

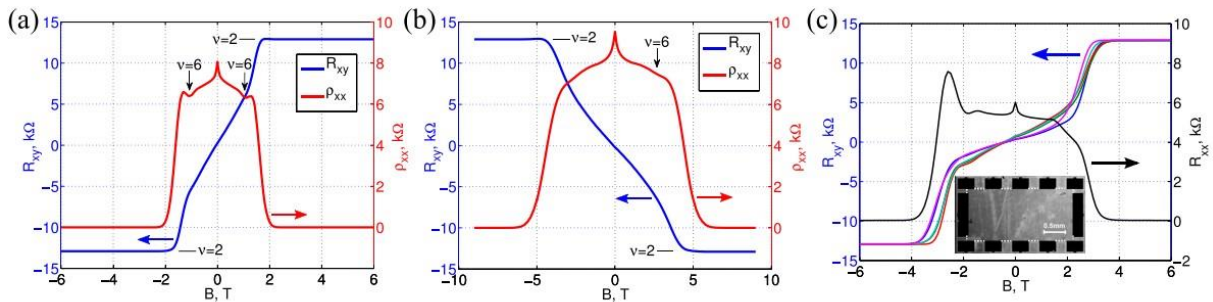


Fig. 6. Low temperature magneto-transport on SiC/G exposed to corona ions. (a) QHE observed for electron doping reveals the monolayer nature of device. (a) ($30 \times 180 \mu\text{m}^2$) at $T = 2 \text{ K}$. (b) QHE in the same device for p-doping, achieved with the corona discharge. (c) Carrier density control by corona ions in millimetre-sized device ($1.25 \times 2.5 \text{ mm}^2$). Inset: Optical microscope (transmission) image of the device, scale bar is 0.5 mm; contacts appear as dark rectangles and the edge of the graphene device is indicated with a dashed line. The onset of hi-QHE occurs at magnetic field B of 4 T for all Hall probes

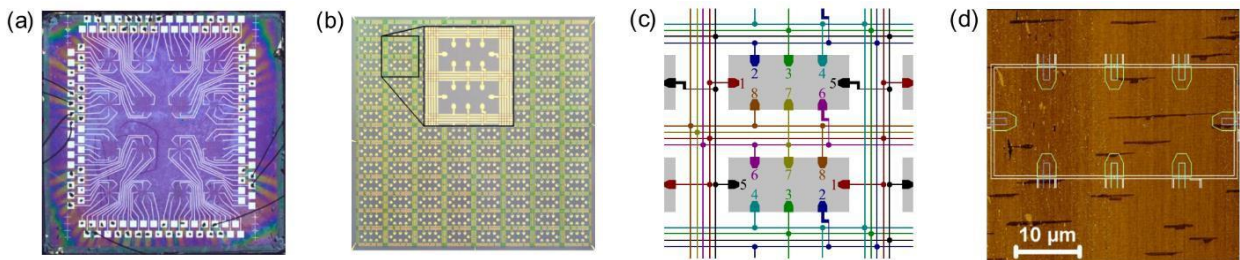


Fig. 7 (a) A microphotograph of the entire chip with 4X4, 6X6 and 10X10 Hall bar arrays. (b) A microphotograph of an array of 100 Hall bars. (c) A part of the schematics of the array. The interconnecting wires are arranged with a significant redundancy. (d) A typical AFM phase image of the graphene substrate with the drawing of a Hall bar on top of it. Dark areas are the bilayer patches.

- Arrays of 100 Hall bars connected in parallel on epitaxial graphene (Fig. 7) were fabricated. One out of four devices has shown quantised resistance that matched the correct value of $R_K/200$ within a measurement precision of 10^{-4} at magnetic fields between 7 and 9 T.

One of the important discoveries during the project was the role of bilayer patches in the Hall bar devices. If a bilayer patch isolates a contact from the other contacts, this contact will have a high resistance, resulting in poor performance as a QHR standard. In order to ensure proper operation of the QHR device, there must be an uninterrupted monolayer path between the contacts (or at least between the voltage contacts). Another important discovery was that it is possible to distinguish bilayer patches in an optical microscope, using real-time digital image enhancement.

This means it is now possible to evaluate graphene quality relatively quickly when fabricating a new device, and possibly take into account the bilayer distribution when patterning the device. A new contact design has also been introduced in order to minimise the probability of poor contacts, even with a relatively high bilayer content in the material. Fig. 8 illustrates how bilayers are detected, and the improved contact design.

The carrier density of graphene is in general not controlled during fabrication, and often ends up too high for QHR measurements. Therefore, some adjustment of the carrier density is needed before measurements are performed. Several different methods were tried with various success. The most successful ones were photochemical gating, ammonia chemical gating and corona discharge (CD) gating, and all these methods have been used successfully by several partners in the project.

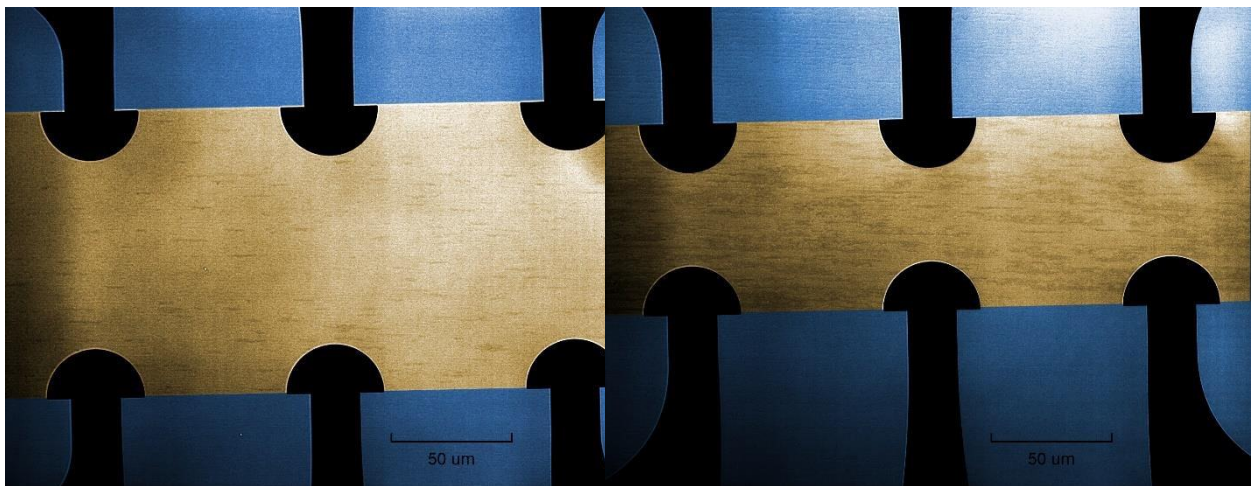


Fig. 8 False colour optical transmission microscope images of graphene Hall bars (beige) from different devices on the same chip. The bilayer content (darker areas) is visible thanks to digital contrast enhancement, and varies across the chip. Blue areas are SiC substrate and black areas are the metal contacts. The contacts are extending into the rectangular area of the Hall bar in order to minimise the risk that bilayer patches isolate the contacts.

The corona discharge method involves a device which generates ionised air molecules by the high voltage corona effect. When the ions settle on the chip surface (the graphene is covered by a thin protective polymer film), they form an electrostatic gate for the graphene, modifying the carrier density. This gate evaporates or leaks away in room temperature after some hours or days, but once the chip is cooled down in the QHR cryostat, the gate is stable as long as it stays cold.

During the carrier density tuning procedure, the ionised air molecules hit not only the chip surface, but also the connecting metal leads, charging them to a high voltage. If the charge is dissipated through the graphene the device may be destroyed, as illustrated in Fig. 9. One should therefore monitor the Hall bar resistance using a source-meter in voltage sourcing mode, and using all the Hall bar contacts. This way, all the leads are connected to low impedance and any excess charge is safely dissipated.



Fig. 9 Left: Carrier density tuning of graphene using a corona discharge device (the blue “gun”). The Hall bar resistance is monitored during the tuning procedure with a sourcemeter in voltage sourcing mode, using all the contacts of the Hall bar. Right: During the tuning procedure, the resistance of this device was monitored with a multimeter, using only the left and right contacts while the remaining contacts were left floating. The device was destroyed by a discharge through the graphene.

3.2 Development of better characterisation methods

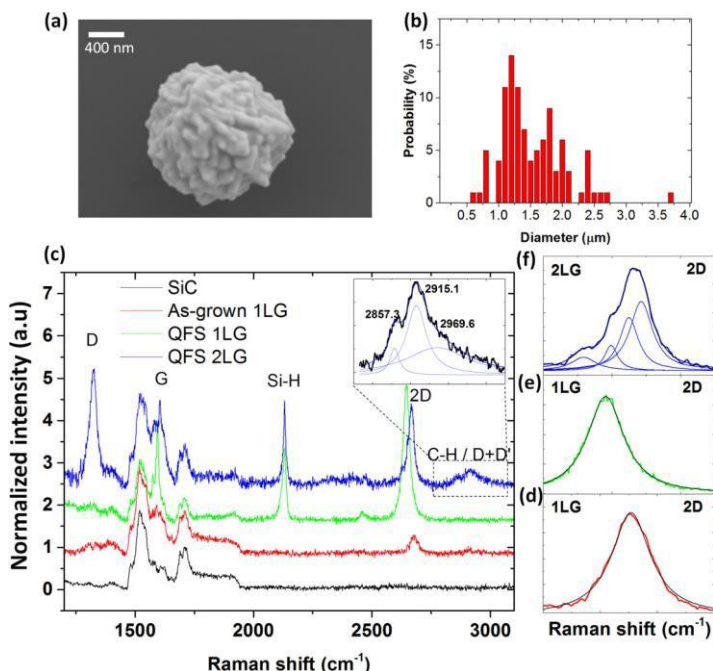


Fig. 10 (a) SEM micrograph of a gold nanoparticle deposited on a graphene sample, (b) statistical analysis of gold nanoparticles, showing median diameter of 1.34 μm , (c) SERS spectra measured on the bare SiC substrate as a reference (black), as-grown 1LG (red), QFS 1LG (green) and QFS 2LG (blue). The enhanced Si-H peak is an indication of successful passivation of the substrate Si atoms with hydrogen and the consequent intercalation of the graphene. The inset in top right shows the fitting of the peak at $\sim 2916\text{ cm}^{-1}$, which corresponds to the C-H bonds and D-D' graphene mode. (d)–(f) 2D fitted peaks of as-grown 1LG, QFS 1LG and QFS 2LG, respectively.

3.2.1 Scanning probe microscopy (SPM) methods

By performing local nanoscale studies of the surface and interface structure of hydrogen intercalated graphene on 4H-SiC(1000) NPL investigated the effect of doping, defects and edges in epitaxial graphene (EG). They showed that intercalation of the interfacial layer results in the formation of quasi-free standing one-layer graphene (QFS 1LG) with change in the carrier type from n- to p-type, accompanied by a more than four times increase in carrier mobility. They demonstrated that surface enhanced Raman scattering (SERS) reveals the enhanced Raman signal of Si-H stretching mode, which is the direct proof of successful intercalation (Fig. 10). Furthermore, the appearance of D, D+D' as well as C-H peaks for the quasi-free standing two-layer graphene (QFS 2LG) suggests that hydrogen also penetrates in between the graphene layers to locally form C-Hsp³ defects that decrease the mobility. Thus, SERS provides a quick and reliable technique to investigate the interface structure of graphene, which is in general not accessible by other

conventional methods.

NPL also compared the three most commonly used scanning probe techniques to obtain a reliable value of the work function in graphene domains of different thickness. The surface potential (SP) of graphene was directly measured in a Hall bar geometry via a combination of electrical functional microscopy and spectroscopy techniques. This enables calibrated work function measurements of graphene domains in ambient conditions and values $W_{1LG} = 4.55 \pm 0.02$ eV and $W_{2LG} = 4.44 \pm 0.02$ eV for single- and bi-layer, respectively, were obtained. It was demonstrated that single-pass frequency-modulated Kelvin probe force microscopy (FM-KPFM) provides more accurate measurement of the SP than amplitude-modulated double-pass (AM)-KPFM. The discrepancy between experimental results obtained by different techniques was explained and attributed to particularities of AM-KPFM method, being the less accurate one. Figs. 11 and 12 show examples of such measurements.

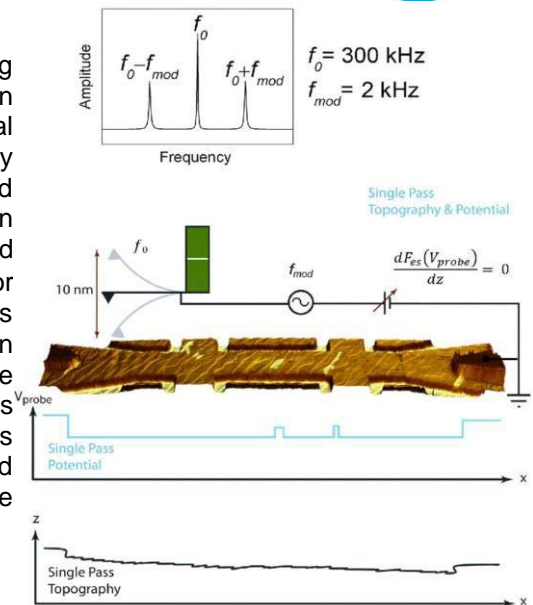


Fig. 11 Schematic diagrams of the FM-KPFM techniques. Topography of the graphene Hall bar is superimposed with SP maps on a 3D image. Plots show characteristic profiles: SP on top and topography on bottom.

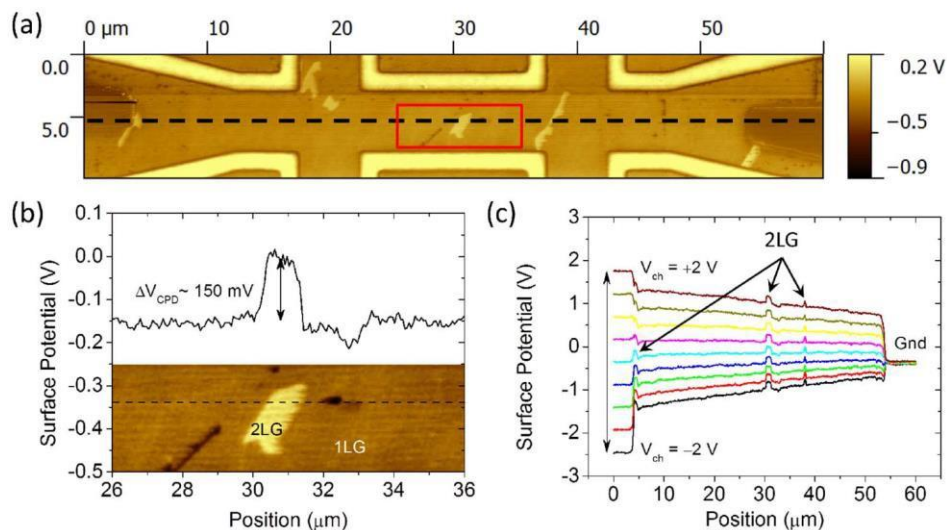


Fig. 12 Surface potential mapping with FM-KPFM. (a) FM-KPFM surface potential map of the grounded Hall bar device. (b) Plot of the surface potential between areas of 1LG and 2LG within the channel along the dashed line shown in the inset. Inset shows the magnified area of the FM-KPFM surface potential map framed in (a). (c) Plot of the surface potential measured between gold leads through the centre of the channel along the line depicted in (a), the left gold lead is biased at V_{ch} between -2 and +2 V and the right gold lead is grounded.

Using local scanning electrical techniques, edge effects in side-gated Hall bar nano-devices made of EG were studied (Fig. 13). It was demonstrated that lithographically defined edges of the graphene channel exhibited hole conduction within the narrow band of 60–125 nm width, whereas the bulk of the material was electron doped. The effect was the most pronounced when the influence of atmospheric contamination is minimal. It was also shown that the electronic properties at the edges can be precisely tuned from hole to electron conduction by using moderate strength electrical fields created by side-gates. However, the central part of the channel remains relatively unaffected by the side-gates and retained the bulk properties of graphene.

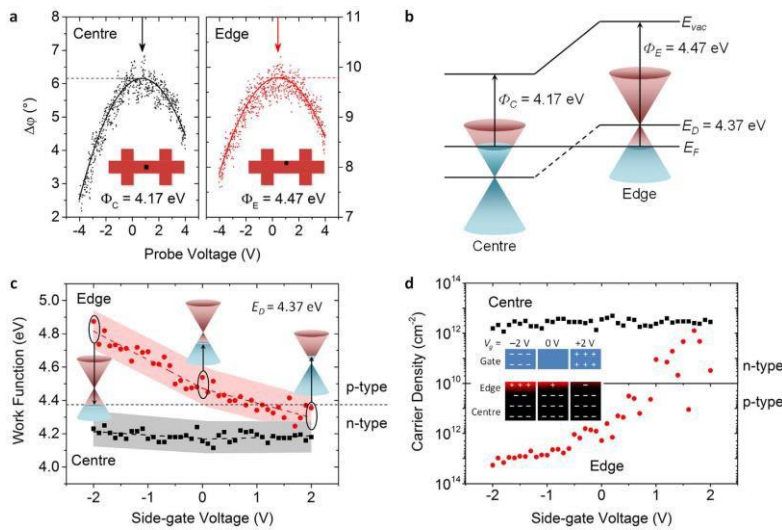


Fig. 13 Quantification of the edge effects. (a) EFS measurements performed on device at the centre and ~ 30 nm away from the edge of the graphene channel. (b) Schematics of the band diagram for 1LG showing the Fermi energy and work function at the centre and edge of graphene channel at $V_g = 5.0$. Dependence of the (c) work function and (d) carrier density on the side-gate voltage at the centre (black squares) and ~ 30 nm away from the edge (red circles) of the channel. The inset in (c) shows a schematic of the band diagram for 1LG at the edge of the channel at different V_g . The inset in (d) shows a schematic of the charge distribution at the centre and edge of the channel.

To analyse graphene films in respect to the number and distribution of layers, NPL further investigated the local surface potential and Raman characteristics of as-grown and ex-situ hydrogen intercalated quasi-free standing graphene on 4H-SiC(0001) grown by chemical vapour deposition (Fig. 14). Upon intercalation, transport measurements revealed a change in the carrier type from n- to p-type, accompanied by a more than three-fold increase in carrier mobility, up to $\mu_h \approx 4540 \text{ cm}^2 \text{ V}^{-1} \text{ s}^{-1}$. On a local scale, KPFM provided a complete and detailed map of the surface potential distribution of graphene domains of different thicknesses. Rearrangement of graphene layers upon intercalation to $(n+1)$ -LG, where n is the number of graphene layers (LG) before intercalation, was demonstrated. This was accompanied by a significant increase in the work function of the graphene after the H₂-intercalation, which confirmed the change of majority carriers from electrons to holes. Raman spectroscopy and mapping corroborated surface potential studies.

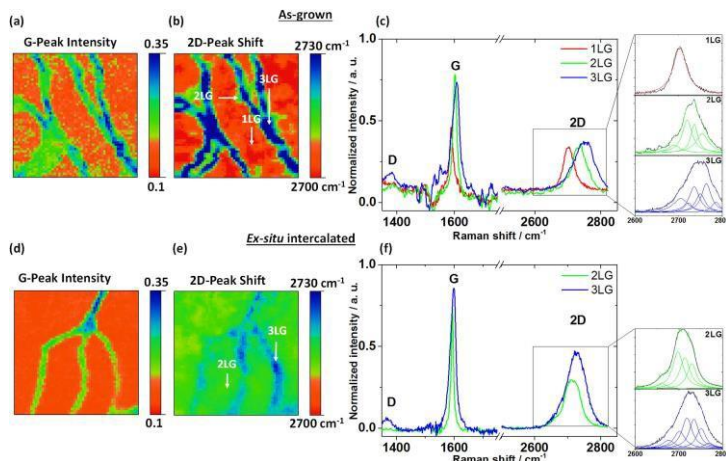


Fig. 14 Raman maps and spectra of as-grown and H₂-intercalated graphene. Raman maps ($10 \times 10 \mu\text{m}^2$) of the G peak intensity (a and d) and 2D peak shift (b and e) for the as-grown (a and b) and intercalated (d and e) samples. Raman spectra taken on the terrace and edges showing: (c) for as-grown sample; 1LG, 2LG and 3LG are depicted with red, green and blue lines, respectively; (f) for intercalated sample; 2LG and 3LG are depicted with green and blue lines, respectively. The insets in (c) and (f) show the selected 2D peaks fitted with Lorentzians.

It was possible to directly correlate the local (20 nm scale) and global electronic properties of a device containing mono-, bi- and tri-layer EG domains on 6H-SiC(0001) by simultaneously performing local surface potential measurements using KPFM and global transport measurements. Using well-controlled environmental conditions, the doping effects of N₂, O₂, H₂O and NO₂ at concentrations representative of the ambient air were investigated. It could be shown that presence of O₂, H₂O and NO₂ led to p-doping of all EG domains. However, the thicker layers of EG are significantly less affected. Furthermore, it could be demonstrated that the general consensus of O₂ and water vapour present in ambient air providing majority of the p-doping to graphene was a common misconception. NPL experimentally showed that even the combined effect of O₂, water vapour, and NO₂ at concentrations higher than typically present in the atmosphere did not fully replicate p-doping from ambient air. Thus, for EG gas sensors it is essential to consider naturally occurring environmental effects and properly separate them from those coming from

targeted species. Figs. 15 to 17 highlight some of those results.

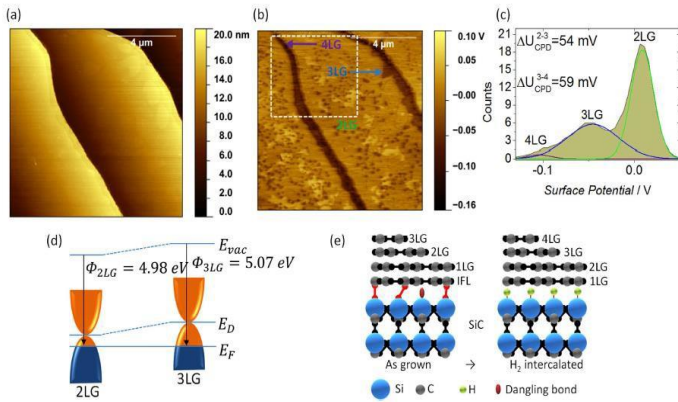


Fig. 15 Topography, surface potential and work function measurements of the H_2 -intercalated graphene. (a) Topography and (b) surface potential map of the ex-situ intercalated graphene sample, showing terraces covered with continuous 2LG, 3LG islands and elongated 3LG and 4LG at the terrace edges. (c) Surface potential histogram of the framed area in (b) fitted with three components, corresponding to 2LG, 3LG and 4LG. (d) Schematic representation of energy band diagrams for 2LG and 3LG. (e) Schematic representation of the transformation of the as-grown graphene layer structure to quasi-free standing graphene.

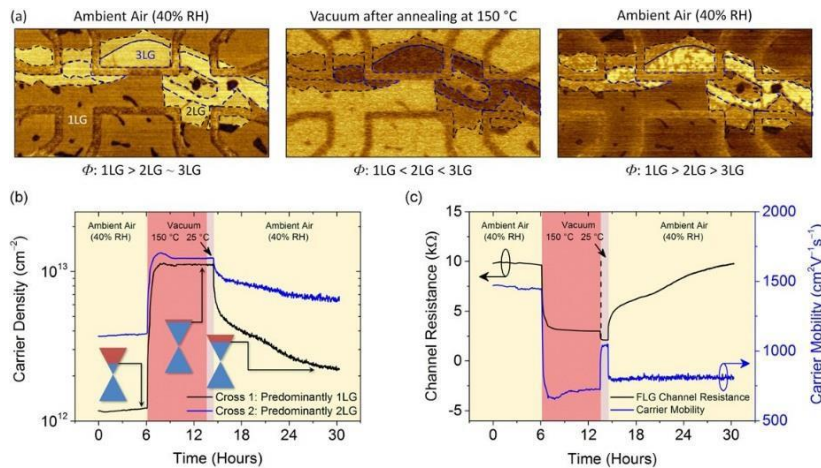


Fig. 16 Surface potential and global transport properties of the Hall bar device in ambient air–vacuum annealing–ambient air. (a) Individual surface potential maps (400 mV colour scale) for ambient air, vacuum after annealing and ambient air. The scan size is $6 \times 3 \mu m^2$. Dashed lines mark 1-2-3LG domains. (b) 1LG and 2LG carrier densities, and (c) few-layer graphene (FLG) channel resistance and carrier mobility in the controlled environments. All measurements were performed at 25 °C.

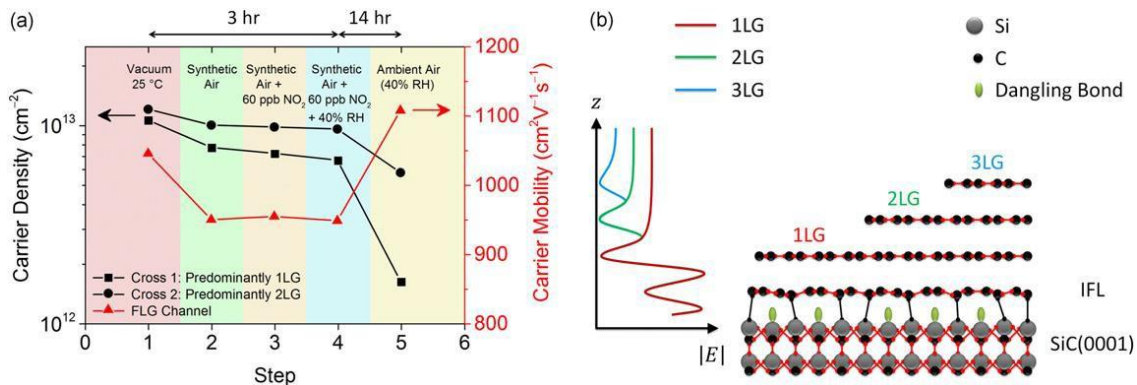


Fig. 17 (a) Measurements of 1LG and 2LG carrier density and FLG carrier mobility in vacuum, synthetic air, 60 ppb NO_2 , 60 ppb NO_2 with 40% relative humidity and ambient air. (b) Schematic representation of the electric field between the epitaxial graphene layers as a result of n-doping from the interfacial layer (IFL).

3.2.2 **Microwave characterisation methods**

A microwave dielectric resonator system has been designed and constructed for the purpose of measuring transport properties of graphene samples. A compact loop oscillator has been developed, including LabVIEW operating software. It has been used to measure a variety of samples up to sizes of greater than 20mm. The design was chosen to be applicable to large scale high quality graphene thin films (especially CVD grown material). Using the microwave resonator, fast measurements of the sheet resistance of graphene samples provided by partners have been carried out and the results sent back to partners. To complete the deliverable concerning measurement in a growth lab the earlier puck design was used (as it was more suitable for small samples such as the epi-films grown at LiU). This was taken to LiU and a number of samples measured in the growth lab.

Non-contact measurement of the sheet resistance of graphene employed a dielectric microwave resonator in a copper housing, close to which the graphene sample could be positioned to allow it to perturb both resonant frequency and Q of the dielectric resonance.

NPL has designed, constructed and tested a simple loop oscillator-based system for microwave resonator measurements to replace the need for expensive vector network analyser instrumentation.

The essence of the loop oscillator operation is that a microwave amplifier is connected between the resonator output port and its input port. The effect is that microwave power thermal fluctuations (which peak at the frequency of the dielectric resonance) are amplified and fed back to be further amplified until the system bursts into spontaneous oscillation at the resonance centre frequency. In addition to a microwave amplifier it is useful to include a fixed frequency bandpass filter centred on the dielectric resonance, an adjustable phase shifter and a fast microwave switch. The equivalent circuit is shown in Fig. 18.

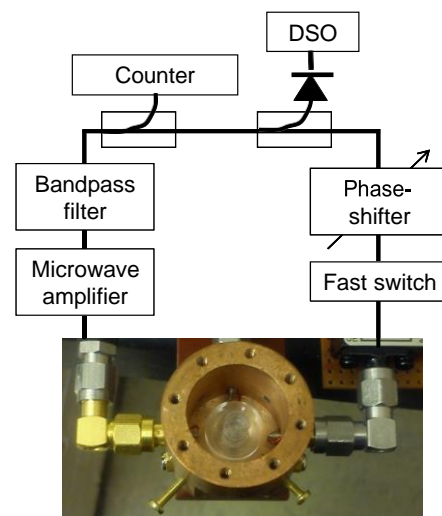


Fig. 18 Schematic of compact loop oscillator with external microwave counter and fast ADC. An image of a resonator is shown at the bottom.

To extend the loop oscillator principle to cover larger samples, as were becoming commonly produced during the latter stages of this project, a loop oscillator was built, with a resonance at 3.5GHz and a larger housing which could accommodate graphene samples up to 30mm x 30mm. It can also be used in an open resonator configuration where the graphene sample is not enclosed within the housing but is presented to a hole in the top surface of the housing. This arrangement allows larger sheets of graphene to be measured e.g. in a roll to roll growth and transfer production line. The microwave system based on loop oscillator is shown in Fig. 19.

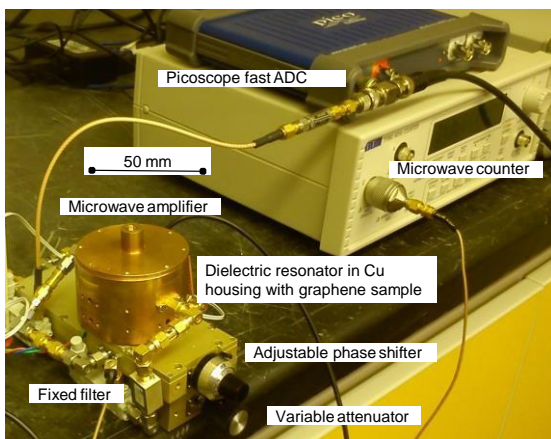


Fig. 19 Image of 3.5GHz loop oscillator, including microwave counter and fast ADC. Note the compact size (illustrated by the 50mm scale bar).

Several samples including SiC epitaxial and CVD graphene provided by the partners have been measured using the microwave system and the results sent to partners. These results have also been reported at several international conferences such as Graphene 2015 and GrapChina 2015 etc., and they were published in [1] and [2].

The electrical properties of a set of SiC graphene monolayer samples were measured, both with the microwave non-contacting method and conventional van der Pauw technique. Also scanned probe measurements using AFM, SKPM and Raman spectroscopy were made on the same films which had been analysed by large scale microwave measurements. The methods show good qualitative agreement. Analysis of the results for the bi-layer coverage ratio of SiC graphene sample using SKPM at local scale was carried out. A paper describing this result has been published in [3] and [4].

3.2.3 *Structural analysis with a liquid crystal texture method*

Large-size graphene synthesised by CVD generally consists of a number of single crystal grains that vary in orientation, size, and shape. Although SEM and AFM images allow determining the shape and size, the orientation of the graphene domain cannot be identified that way. The alignment of a graphene domain, the size of a single domain, the edge type of graphene, and grain boundaries can, however, be analysed using the liquid crystal (LC) texture method developed at KRISS. In this method, liquid crystals align parallel to the carbon rings and can orient into three symmetric directions. The birefringence of the liquid crystal provides information about the graphene domain size, its orientation, and boundaries.

The employed LC was 4-cyano-4-pentylbiphenyl (5CB) which is nematic at room temperature. 5CB is known to be aligned along a specific direction on graphene. The LC texture was observed using a reflection mode of a polarising optical microscope. The Berek compensator was used to determine the LC direction orientation. The LC cells were constructed using a glass substrate and a Cu foil. The cell gap was adjusted within a few micrometres and was fixed using epoxy resin. The glass substrate was treated by lecithin for homeotropic alignment. The LC was injected into the cell at an isotropic phase at high temperature. Afterwards, the temperature was subsequently cooled to room temperature for observation.

The LC textures on graphene films show small and large grains on the CVD graphene films. Each grain is a single crystal. However, the LC texture shows brightness variation under the polarising microscope for different crystal orientations due to the random orientation of the grains. LC aligns along 3 symmetry directions of graphene. Therefore, three regions should appear alternately with dark (or bright) regions when the sample is rotated by 60°. However, the LC texture showed distinct regions with different rotation angles deviating from 60°. The LC texture shows changes of direction at the grain boundaries and can be assigned to the distinct grains. The change of texture at grain boundaries was evidenced by Raman spectra observed at different positions on the graphene. The central frequencies of the 2D band and the LC texture at the inner regions are different from that at the boundary regions. The frequency and intensity of the Raman measurements for the inner positions of graphene are independent of location, but they vary at the boundary locations. The central frequency of the 2D band shifted to smaller frequencies due to stress in the crystal.

The graphene islands do not form a single grain with a uniform crystal structure. They consist of several regions that are oriented along different directions. The crystal orientation of every lobe can be mapped. The distributions are similar to the crack of Cu grains and related to the underlying Cu substrate. Disordered structure such as cracks and wrinkles are observed. The cracks are caused by the Cu foil. Patterns of fine repeating lines were fragile and could be rubbed out by using an eraser. The LC texture suggests that the cracks and wrinkles occur after graphene growth.

Most graphene grains consist of not only a uniform single layer but also show multilayer regions. Generally, the multilayers are found in the central regions. The bilayer graphene existing in the central regions is rotated by 30° with respect to the bottom single layer. From the LC texture, small regions of a 2nd graphene layer (in bilayer form) are located on top of the uniform single graphene layer.

The size and shape of the graphene grains, crystal orientation, type of domain boundaries, cracks, and wrinkles are examined by analysing the direction orientation using a polarising microscope. The LC texture method is an easy and reliable way to show the domain orientation and edge type of graphene on the macroscopic scale.

3.3 Exploration of the limits of graphene in precision resistance metrology

3.3.1 Pre-selection of devices by low-temperature magneto-resistance measurements

In order to evaluate the practical potential of graphene for QHR measurements, at RISE comparisons were performed between graphene devices and standard GaAs based QHR devices.

The first practical difference is the carrier density tuning which is required for graphene devices. Although one may have a device with a suitable carrier density to start with, it can still be useful to find the optimal density in terms of magnetic field or critical current. Chips were tested several times with different carrier densities, each time cooling it and measuring the longitudinal resistance as a function of magnetic field. This resistance needs to be essentially zero for QHR measurements to be accurate. The results from one of the chips is shown in Fig. 21. It was found that the difference in tuning the resistance between a working device (1.80 k Ω) and a non-working device (1.85 k Ω) can be quite small, but reproducible. Once a particular device has been characterised and the optimum tuning resistance is known, the tuning procedure takes only minutes to perform. The lowest usable magnetic field for precision measurements with this device was 6.5 T, which is considerably lower than the 8 T – 11 T needed for GaAs devices. Other devices can have even lower minimum usable fields, but they require a very homogeneous carrier density in the Hall bar. In particular, the bilayer content needs to be very low, since the bilayer patches affect the carrier density around them.

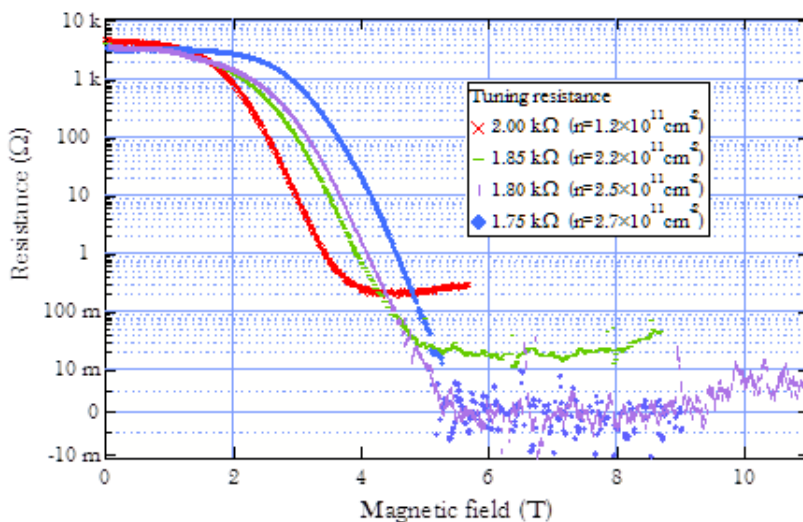


Fig. 1 After tuning the resistance using the corona discharge method, the sample was cooled and the longitudinal resistance was measured as a function of magnetic field. This resistance needs to be vanishingly small for QHR measurements. The graph shows four measurements with the same device, after tuning the resistance to different levels. Two of the curves reached the noise floor, and could be used for precision QHR measurements.

Actual resistance calibrations were done using a cryogenic current comparator and the graphene and GaAs QHR devices. The results (see Fig. 20) show good agreement, and it can be concluded that the graphene devices offer several advantages. First, they can be used at 4.2 K, while the GaAs device needed to be cooled to 2 K or lower. The graphene devices are fully quantised at 4.2 K, while for GaAs sometimes even 1.5 K is not low enough. Further, the system can be operated at a lower magnetic field. Finally, the graphene devices support a higher measurement current than the GaAs devices, which means a lower noise level.

At RISE it was found that just switching to graphene QHR devices in an existing measurement setup already offers considerable advantages. It saves time and helium by operating at higher temperature, and yields a lower measurement uncertainty thanks to the superior properties of graphene. The expanded ($k=2$) uncertainty of calibrating a 10 k Ω resistance standard decreased by a factor of 3, from 25 n Ω/Ω to 8.4 n Ω/Ω . Many other smaller NMIs have systems comparable to that at RISE, and they will be able to improve their systems in a similar way.

SIB51 GraphOhm

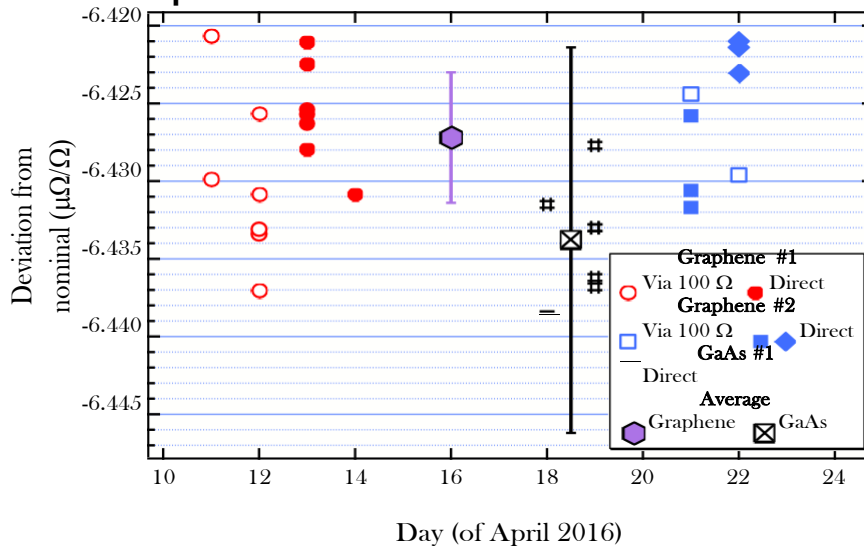


Fig. 20 The results of calibrating a 10 k Ω resistor against graphene and GaAs QHR standards. Both direct measurements against QHR and measurements against a 100 Ω resistor calibrated against QHR are included. Error bars are standard uncertainty bars.

According to F Delahaye and B Jeckelmann “Revised technical guidelines for reliable dc measurements of the quantised Hall resistance” non-ideal contacts to the 2DEG are often the major device-related limitation encountered by metrologists. Poor contacts are characterised by a high contact resistance and in the worst case by a non-linear behaviour. It is therefore essential to investigate the properties of the metal contacts to the graphene layer and produce them in a controllable way.

NPL has investigated Ti/Au contacts to monolayer epitaxial graphene on SiC (0001). Using three-terminal measurements in the quantum Hall regime they observed variations in contact resistances ranging from a minimal value of 0.6 Ω up to 11 k Ω . They identified bilayer graphene interruptions to the quantum Hall current as a major source of high-resistance contacts, whilst the effects of interface cleanliness and contact geometry could be discarded. Moreover, methods to improve the reproducibility of low resistance contacts (< 10 Ω) suitable for high precision quantum resistance metrology were experimentally demonstrated.

A major limitation of the epitaxial graphene on SiC (SiC/G) technology so far has been the high carrier concentration of the as-grown material, which makes it difficult to tune to the range where the QHE is observed at relatively low magnetic field. Conventional electrostatic gating using metal gates has been used in graphene FETs, but fails in metrological applications because of the electron leakage through the gate dielectric, which affects precision measurements. The solution has been found in ionic gating as ions are much less mobile. Reversible carrier density control across the Dirac point in epitaxial graphene on SiC (SiC/G) was demonstrated via high electrostatic potential gating with ions produced by corona discharge. The method, developed by partner Chalmers, is attractive for applications where graphene with a fixed carrier density is needed, such as quantum metrology, but also more generally as a simple method of gating 2DEGs formed at semiconductor interfaces and in topological insulators.

3.3.2 Influence of Disorder and robustness

Physics of the disordered Dirac point in epitaxial graphene

When the carrier concentration in graphene is made very low, close to the Dirac point, the sea of charge carriers is broken into the puddles of electrons and holes by the electrostatic potential disorder in the underlying substrate. NPL performed a study of these disorder effects on epitaxial graphene in the vicinity of the Dirac point by magnetotransport. Hall effect measurements showed that the carrier density increases quadratically with temperature, in good agreement with theoretical predictions which take into account intrinsic thermal excitation combined with electron-hole puddles induced by charged impurities. Disorder strengths in the range 10.2–31.2 meV can be deduced, depending on the sample treatment. By investigating the scattering mechanisms, the impurity density was estimated to be $3.0\text{--}9.1 \times 10^{10} \text{ cm}^{-2}$ for the samples studied. A scattering asymmetry for electrons and holes was observed, which is consistent with theoretical calculations for graphene on SiC substrates. NPL could also show that the minimum conductivity increases with increasing disorder strength, in good agreement with quantum-mechanical numerical calculations.

Spin influence on quantum coherence

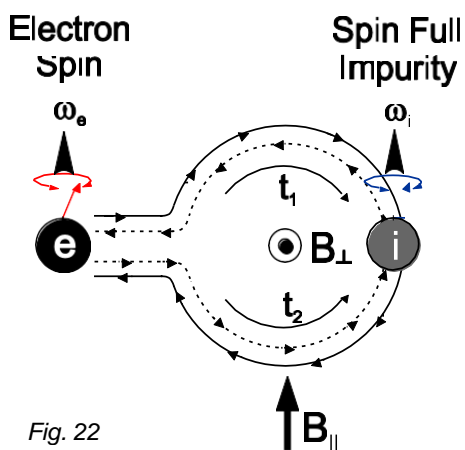


Fig. 22

Quantum interference of the electrons propagating along various paths in a disordered 2D conductor leads to corrections to electrical conductivity at low temperatures. In graphene this interference is generally destructive, so that the electrons tend to localise and the resistance is increased compared to the classical Drude value. This quantum correction is destroyed by weak perpendicular magnetic fields and by the randomising effect of temperature, however it is experimentally seen to stay finite even at the lowest temperatures. What limits the quantum coherence? - is the question that we wanted to address by our new study.

In one of our previous publications we have cautiously put forward an idea that the coherence may be limited by scattering on spinful defects. Now we were able to prove this idea directly by applying a moderate in-plane magnetic field which polarised the spins of the defects and suppressed the electron spin relaxation.

Unexpectedly, the influence of the in-plane field was non-monotonic: a very weak in-plane field has resulted in a small but noticeable increase of the electron spin relaxation before it was suppressed in a somewhat stronger field. The behaviour in the weak field was understood in terms of a previously unknown spin dynamics contribution to magnetotransport. In-plane field forces precession of both the electron spin and the impurity spin. If the two rotate at the same rate and in the same direction, precession makes no effect on scattering. However, if electrons 'see' the spin of scattering impurities at random phase, the coherence is suppressed. Fitting the theory to the experimental data allowed us to estimate the g-factor of the defects responsible for decoherence.

3.3.3 Investigating the breakdown mechanism of the quantum Hall effect

Visualisation of weak spots

Bilayer patches in an otherwise monolayer matrix are formed inadvertently when graphene grows epitaxially on SiC by high-temperature sublimation. The role of these inclusions in the QHE regime was not previously known. NPL studied an epitaxial graphene monolayer with bilayer inclusions via magnetotransport measurements and scanning gate microscopy at low temperatures. They found that the same bilayer inclusions can be metallic or insulating depending on the initial and gated carrier density. The metallic bilayers act as equipotential shorts for edge currents in the QHE regime. These bilayers destroy the operation of the QHE resistance standard at high gated carrier densities. The insulating inclusions formed at low carrier densities can be seen as voids in the graphene material and effectively reduce the width of the Hall bar. In very narrow constrictions formed by the bilayers they allow to divert the flow of electrons by the local electrostatic field of the scanning gate electrode. Either way, the large inclusions that straddle the Hall bar should be avoided.

Breakdown of the quantum Hall effect in epitaxial graphene at low fields and elevated temperatures

Having established a reliable way to tune the carrier density and developed understanding of the influence of disorder at low carrier densities, NPL investigated the phase space defined by the quantum Hall effect breakdown in polymer gated epitaxial graphene on SiC (SiC/G) as a function of temperature, current, and magnetic field. They found that at 2 K, breakdown currents (I_c) in graphene are almost 2 orders of magnitude higher than in GaAs devices. As described in the following sections, this knowledge was used to explore the potential of using graphene as a high temperature (> 2 K) and low magnetic field (< 5 T) quantum resistance standard.

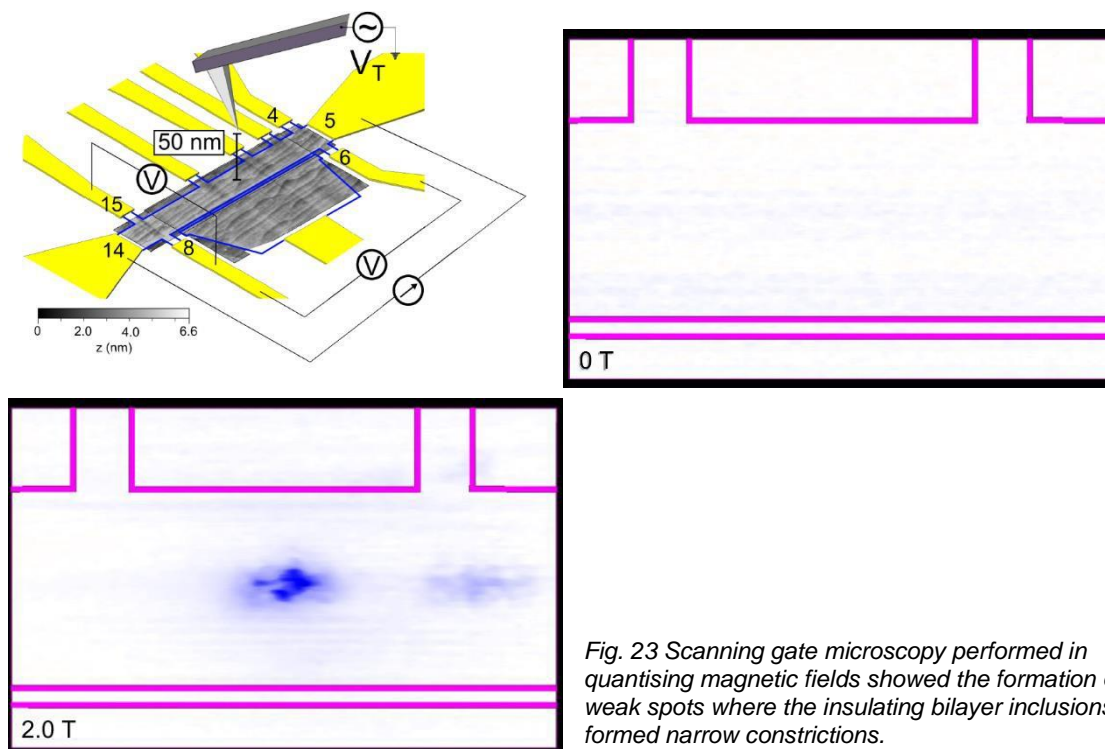


Fig. 23 Scanning gate microscopy performed in quantising magnetic fields showed the formation of the weak spots where the insulating bilayer inclusions formed narrow constrictions.

3.3.4 Evaluating the optimal quantisation conditions

Energy relaxation of hot electrons

Electrons are injected into a 2DEG sample from the metal electrodes at high energy of the order of μR_k above the Fermi level and they have to thermalise quickly to sustain high breakdown current. Previously NPL had studied the energy relaxation of hot Dirac fermions in monolayer epitaxial graphene and concluded that it occurs very quickly compared to conventional semiconductor 2DEGs, on the time-scale of picoseconds. This is a major factor supporting high QHE breakdown currents alongside very high cyclotron frequencies. In this project the energy relaxation of hot Dirac fermions in bilayer epitaxial graphene was experimentally investigated by magnetotransport measurements on Shubnikov–de Haas oscillations and weak localisation. The hot-electron energy loss rate was found to follow the predicted Bloch–Grüneisen power-law behaviour of T^4 at carrier temperatures from 1.4 K up to ~ 100 K, due to electron-acoustic phonon interactions with a deformation potential coupling constant of 22 eV. A carrier density dependence $n^{-1.5}$ in the scaling of the T^4 power law is observed in bilayer graphene, in contrast to the $n^{-0.5}$ dependence in monolayer graphene, leading to a crossover in the energy loss rate as a function of carrier density between these two systems. The electron–phonon relaxation time in bilayer graphene was also shown to be strongly carrier density dependent, while it remains constant for a wide range of carrier densities in monolayer graphene. The results and comparisons between the bilayer and monolayer exhibit a more comprehensive picture of hot carrier dynamics in graphene systems.

Giant quantum Hall plateaus

NPL performed measurements of the quantum Hall effect in epitaxial graphene showing the widest quantum Hall plateau observed to date extending over 50 T, attributed to an almost linear increase in carrier density with magnetic field. This behaviour is strong evidence for field dependent charge transfer from charge reservoirs with exceptionally high densities of states in close proximity to the graphene. Using a realistic framework of broadened Landau levels, the densities of donor states were modelled and the field dependence of charge transfer was predicted in excellent agreement with experimental results, thus providing a guide towards engineering epitaxial graphene for applications in quantum metrology.

Demonstration of the QHE at low magnetic field and elevated temperature

Once the phase space for operation of graphene in the QHE regime was established, NPL were able to optimise the zero-field carrier density of the Hall bar to provide the highest possible breakdown current for operation at 5 T magnetic field. This is non-trivial, because the effective carrier density depends on the field

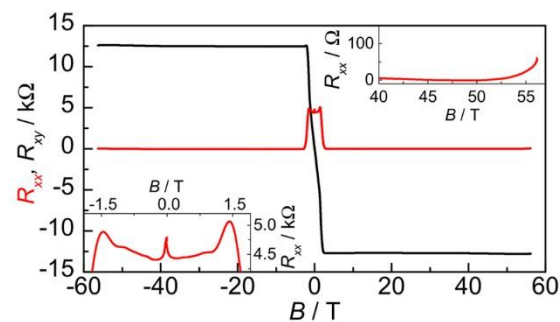
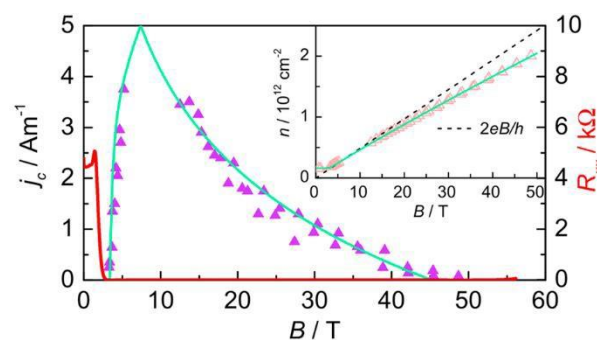


Fig. 24 Pulsed magnetic field measurements of the quantum Hall effect in epitaxial graphene on SiC at $T = 2$ K as observed in the longitudinal resistance (R_{xx} , red) and Hall resistance (R_{xy} , black) showing an exceptionally wide (~ 50 T) $\nu = 2$ plateau. Upper inset: The end of the plateau at $B > 50$ T. Lower inset: R_{xx} at low magnetic fields showing clear Shubnikov-de Haas oscillations and weak localisation.



Magnetic field dependence of the breakdown current (purple triangles) for the $\nu = 2$ plateau and a best fit (solid line) using the new theory. The red line shows the longitudinal resistivity and the inset shows the corresponding magnetic field dependent carrier density.

due to the charge transfer described above, but also depends on the operation temperature. Finally, NPL demonstrated quantum Hall resistance measurements with metrological accuracy in a small cryogen-free system operating at a temperature of around 3.8 K and magnetic fields below 5 T. Operating this system requires little experimental knowledge or laboratory infrastructure, thereby greatly advancing the proliferation of primary quantum standards for precision electrical metrology. This significant advance in technology has come about as a result of the unique properties of epitaxial graphene on SiC.

Looking into the future. Quantum hall arrays.

Single Hall bars made of graphene have already surpassed their state-of-the-art GaAs based counterparts as an $R_K/2$ standard, showing at least the same precision and higher breakdown current density. Compared to single devices, quantum Hall arrays using parallel or series connection of multiple Hall bars can offer resistance values spanning several orders of magnitude and (in case of parallel connection) significantly larger measurement currents, but impose strict requirements on uniformity of the material. To evaluate the quality of the available material, we have fabricated arrays of 100 Hall bars connected in parallel on epitaxial graphene. One out of four devices has shown quantised resistance that matched the correct value of $R_K/200$ within the measurement precision of 10^{-4} at magnetic fields between 7 and 9 T. The defective behaviour of other arrays is attributed mainly to non-uniform doping. This result confirms the acceptable quality of epitaxial graphene, pointing towards the feasibility of well above 90% yield of working Hall bars.

Measurements on CVD graphene

Fig.26-Left reports on the conductance $G_{xx} = 1/R_{xx}$ as a function of the gate voltage V_g at 0.3 K in a 200 μm -wide CVD sample, measured at LNE. The charge neutrality point (CNP) is positioned at $V_g = 3.5$ V, indicating a residual hole density of $2.6 \times 10^{11} \text{ cm}^{-2}$. At high carrier density (about $1 \times 10^{12} \text{ cm}^{-2}$), the hole (electron) mobility is about $3\,100 \text{ cm}^2 \text{ V}^{-1} \text{ s}^{-1}$ ($2\,300 \text{ cm}^2 \text{ V}^{-1} \text{ s}^{-1}$). The Hall resistance, R_H , measured at 0.3 K and 19 T, shown as a function of V_g in the lower part of Fig.26 Left, features well-developed plateaus at values $R_K/2$ and $R_K/6$ which coincide with the minima of the longitudinal resistance R_{xx} . Nevertheless, it turns out that R_H is not well quantised, even on the $\nu = -2$ plateau, deviating from $R_K/2$ by more than 1% at a current of $1 \mu\text{A}$, while R_{xx} is higher than 150Ω . To identify the mechanism responsible for this loss of quantisation, G_{xx} and G_{xy} were measured over a large range of ν values, at several temperatures between and 40 K (Fig. 26-Right) and at magnetic fields between 5 and 19 T. The measurements show that G_{xx} follows power-law dependences as a function of temperature (Fig.25-Left), magnetic field and current and not exponential behaviours as would be expected for a dissipation mechanism based on thermal activation or variable range hopping (VRH). This was explained by the presence of a high-density of line defects, such as wrinkles and grain boundaries, forming a continuous network connecting Hall bar edges (Fig.25-Right). Numerical simulations of the transport properties in graphene nano-ribbons have confirmed that quasi-one-dimensional extended non-chiral states can form along line defects and short circuit the chiral quantum Hall edge states along the Hall bar edges. This work, which motivates the investigation of the QHE in large CVD single crystals, was reported in [5]

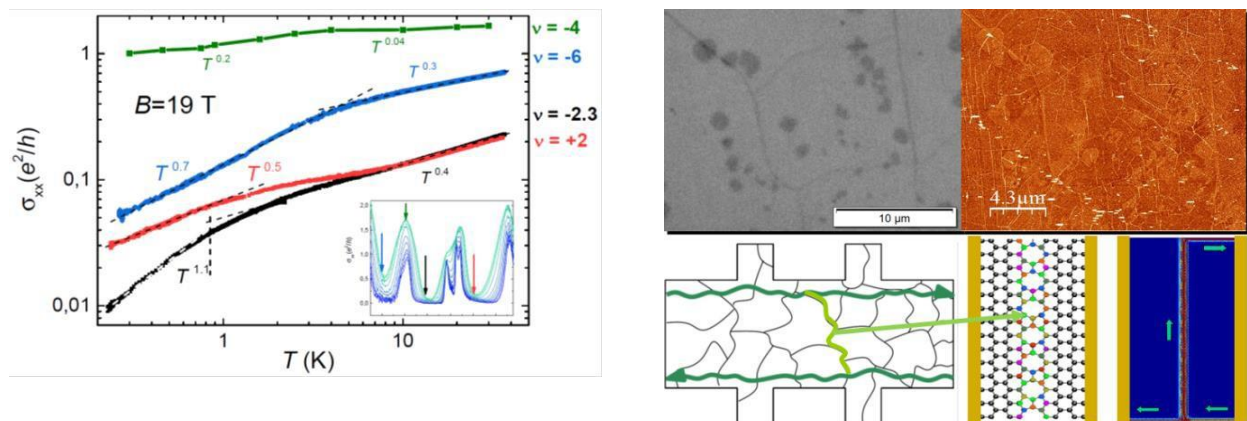


Fig. 25 Left: G_{xx} vs T in log-log scale at 19 T at $\nu = -4, -6, -2.3$ and $+2$. Right: Scanning electron microscopy and atomic force (top-left) microscopy images of the graphene (top-right). Schema representing line defects in the sample (bottom-left). Numerical simulation and visualization of the current flowing along a line defect crossing the sample (bottom-right). Data from [5].

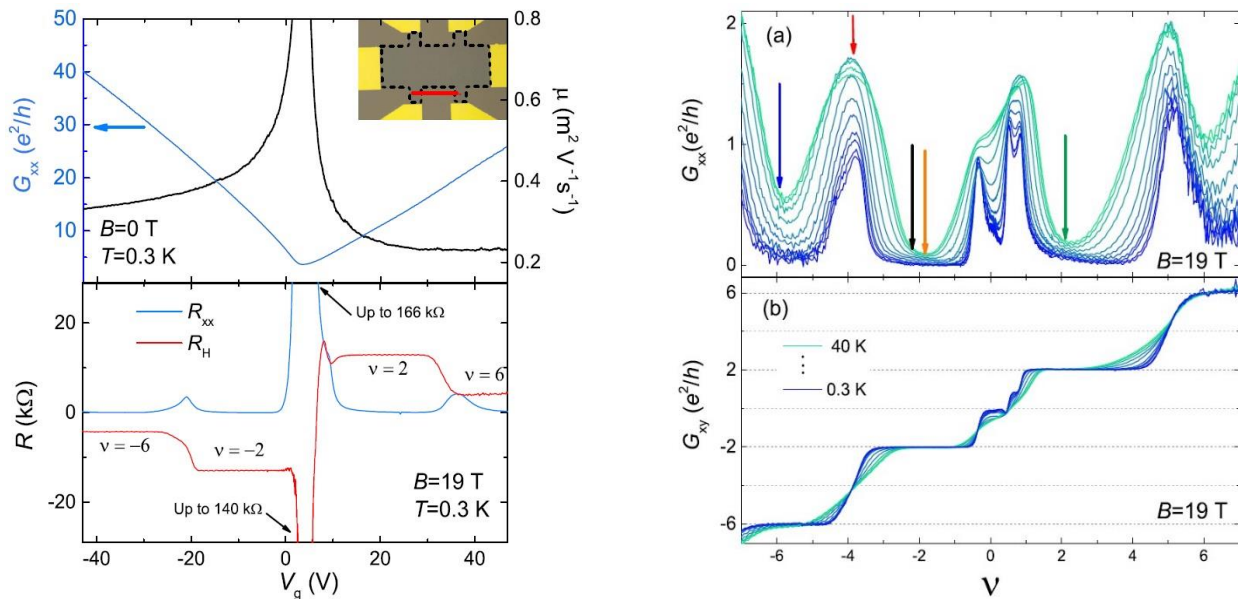


Fig. 26 Left: Longitudinal conductance and carrier mobility vs V_g (upper part) and R_H and R_{xx} vs V_g (lower part). Inset: Hall bar optical image. The length between voltage terminals is 200 μm and equal to the Hall bar width. Right: (a) G_{xx} and (b) G_{xy} vs Landau level filling factor ν for T between 0.3 and 40 K at 19 T. Arrows in (a) indicate the values of ν at which measurements shown in Fig. 2 are performed. Data from [5].

Measurements on SiC-CVD graphene

Two of the SiC-CVD graphene samples described in section “*Epitaxial graphene at LNE*” were deeply investigated. The first one had an electron density of $3.2 \times 10^{11} \text{cm}^{-2}$ at a mobility of $3\,500 \text{cm}^2 \text{V}^{-1} \text{s}^{-1}$. At higher magnetic fields, a wide Hall resistance plateau $R_H/2$ extended from 5 T up to 19 T (Fig. 27-Left: black curve), coinciding with zero R_{xx} (blue curve). The comparison with the narrow $R_H/2$ Hall resistance plateau (green curve) of a conventional GaAs QHR is striking. The quantised Hall resistances measured in the graphene sample and a GaAs reference sample were accurately compared indirectly via a 100 Ω transfer resistor using a cryogenic current comparator (CCC) bridge. The device demonstrated perfect quantisation of the Hall resistance within one part in 10^9 , over a 9 T-wide magnetic field range from 10 T up to 19 T, at 1.4 K (Fig. 27-Left). A mean relative deviation of $(-2 \pm 4) \times 10^{-10}$ was measured between quantised Hall resistances in graphene and in GaAs.

The physics of the quantised Hall resistance plateau was investigated by the characterisation of the dissipation (R_{xx}) dependence on temperature and current (Fig. 27-Right). It turned out that the dissipation is dominated by variable range hopping (VRH) with soft Coulomb gap mechanism. The wide quantised Hall resistance plateau is explained by a localisation length of states at the Fermi energy that remains very close to the magnetic length $l_B = \sqrt{\hbar/eB}$ over a large magnetic field range of 9 T. This is partly caused by a pinning of the Landau level filling factor at $\nu=2$ due to a charge transfer from the donor states in the buffer layer between SiC and graphene. This work was reported in [6].

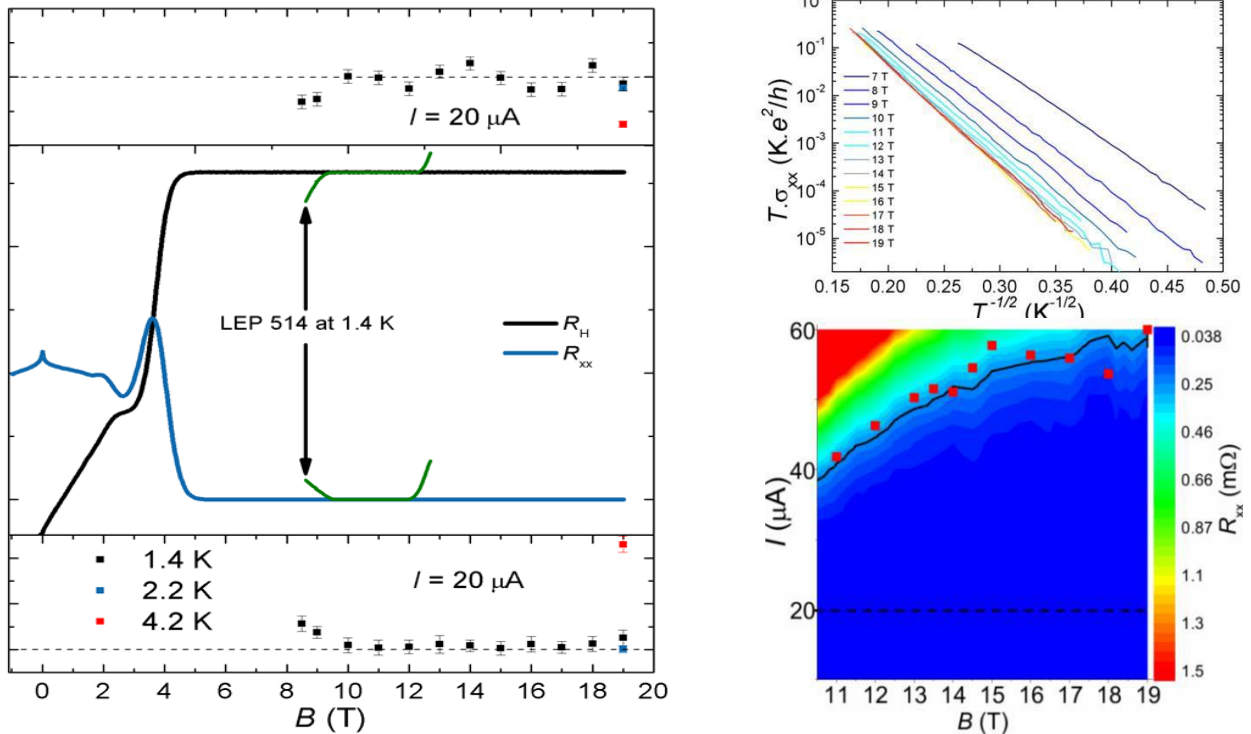


Fig. 27. Left-centre: magneto-resistance characterization of a graphene sample (R_H black, R_{xx} blue) and a GaAs sample (R_H green). Left-top: Relative deviation of the Hall resistance as a function of B , with 1 s.d. error bars. Left-bottom: Longitudinal resistance R_{xx} as a function of B . Right-top: temperature dependence of the conductivity demonstrating the VRH mechanism. Right-bottom: Colour rendering of R_{xx} as a function of the current I and B at $T=1.4$ K (black line corresponds to $R_{xx}=0.25$ m Ω). Black line can be adjusted by $\xi(B)^{-2}$ fitting data (red square) where $\xi(B)$ is the localization length, as expected from VRH mechanism. Data from [6].

The second Hall bar sample, of similar geometry, had a lower carrier density of $1.8 \times 10^{11} \text{ cm}^{-2}$ and was remarkably homogeneous, within $1.5 \times 10^{10} \text{ cm}^{-2}$, and a mobility of $9\,400 \text{ cm}^2 \text{ V}^{-1} \text{ s}^{-1}$. At 1.3 K, the Hall resistance R_H (Fig. 28a) exhibited a wide $R_H/2$ plateau, extending from 2 T up to the maximum accessible magnetic field of 14 T. The contacts at the eight terminals had resistance values below 1 Ω (0.1 Ω for current terminals). The quantised Hall resistance was accurately compared to that in a GaAs reference sample using the CCC-based bridge. The CCC was also used to perform accurate and precise measurements of R_{xx} . Fig. 28-Right reports the relative deviation of the quantised resistances measured in the graphene and GaAs-based samples (a) and R_{xx} (b) in graphene, as a function of the magnetic field B at $T=1.3$ K. No significant deviation is observed from 3.5 T up to 14 T within a relative uncertainty of $1 \cdot 10^{-9}$. This coincides with very low longitudinal resistance values below 40 $\mu\Omega$ over the whole magnetic field range, with minimum value of $5 \pm 2 \mu\Omega$ around 5-6 T. $B=3.5$ T constitutes the lowest quantisation magnetic induction ever achieved by any two-dimensional semiconductor. The homogeneity of the Hall quantisation in the whole device was demonstrated with a $1 \cdot 10^{-9}$ uncertainty by carrying out measurements using three different Hall voltage terminal-pairs.

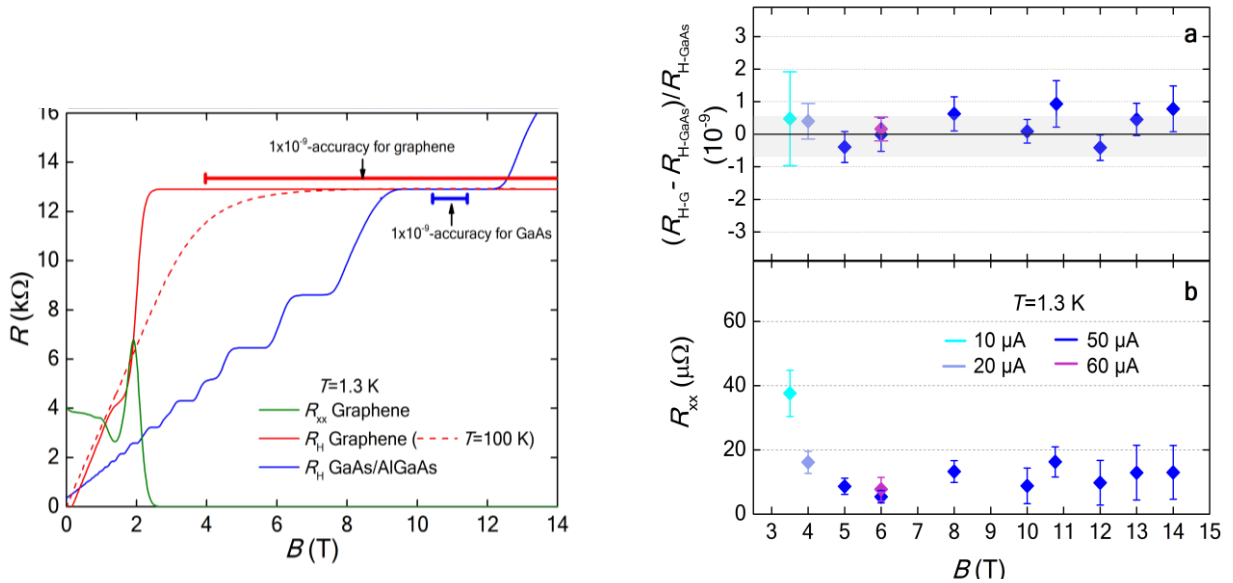


Fig. 28
 a. Magneto-resistance in graphene and GaAs/AlGaAs samples. Data from R. Ribeiro-Palau et al, Nature Nanotechnology, 10, 965 (2015).

b. Relative deviation of the quantized Hall resistance in graphene and GaAs/AlGaAs devices. Longitudinal resistance R_{xx} measured in graphene device. Error bars correspond to 1 s.d.. Data from R. Ribeiro-Palau et al, Nature Nanotechnology, 10, 965 (2015).

Fig. 29-Left and Fig. 29-Right report on the critical temperature T_c and the critical current I_c respectively, below which the quantisation of the Hall resistance was accurate to within 1.10^{-9} , as a function of B . It is shown that the device could be accurately operated at 5 K, 5 T and up to 10 K at 8.5 T. A maximum operating current of 500 μA was achieved at 8 T and 1.3 K. It remains above 250 μA at 5 K. $T_c(B)$ and $I_c(B)$ define the limits of a domain of experimental conditions (B, T, I) in which R_H is accurate to within 10^{-9} , much larger than the one of a GaAs-based quantum resistance standard. The device can therefore be used at magnetic inductions down to 3.5 T, temperatures up to 10 K or currents as high as 500 μA . The working points (5 T, 5 K, 50 μA) or (6 T, 5 K, 160 μA), for example, constitute experimental conditions which are fully compatible with an operation in a cryogen-free QHE setup as the one developed by NPL. The results of this work were published in [7].

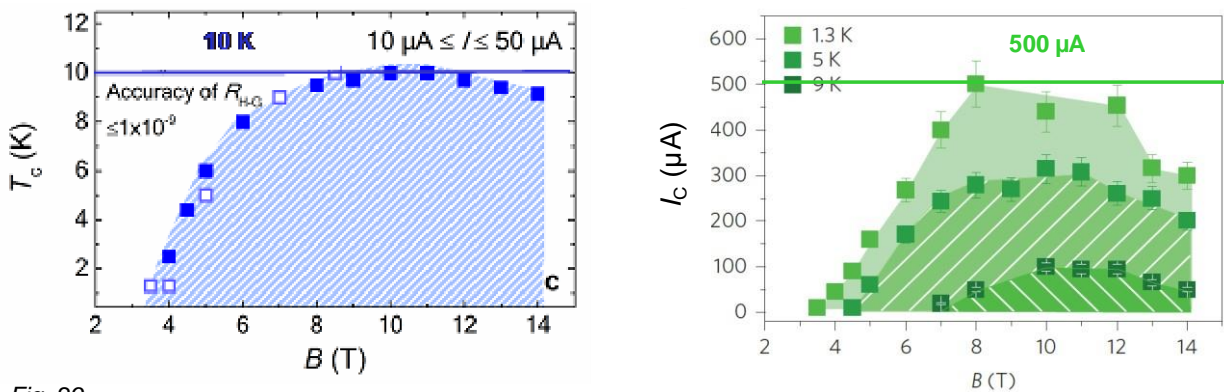


Fig. 29
 a. Critical temperature T_c , below which R_H is accurate to within 10^{-9} , as a function of B . Data from [7].

b. Critical current I_c , below which R_H is accurate to within 10^{-9} , as a function of B . Data from [7].

To conclude, LNE performed metrological measurements of several devices fabricated from graphene grown using different techniques. LNE collaborated with other partners of the project in testing devices patterned by Chalmers University/RISE and made of graphene produced by thermal decomposition of silicon carbide in Linköping University. In polycrystalline CVD graphene grown on copper by the project collaborator *Institut Néel*, an anomalous dissipation mechanism limiting the Hall quantisation was observed and explained by the short-circuiting of the Hall bar edges by extended states existing along line defects (wrinkles or grain boundaries). LNE brought the first demonstration of the perfect quantisation of the Hall resistance in graphene produced by CVD on silicon carbide, a hybrid growth technique developed in CRHEA-CNRS. The physics of the QHE, notably the wide Hall resistance plateau, was investigated owing to accurate and very sensitive measurements. It was then shown that devices based on graphene grown by CVD on SiC could operate in very relaxed experimental conditions, inaccessible to GaAs-based devices. These conditions are compatible with the development of a cryogen-free, compact and low cost QHE setup, enabling the dissemination of the ohm with a quantum-accuracy towards end-users. This opens the way to an easier dissemination of several electrical units, making graphene disruptive in the metrology field. Beyond, the universality test performed with a record uncertainty supports the setting of the future International System of units (SI) based on defining constants, the realisation of which strongly rely on the quantum electrical standards.

Quantum Hall effect measurements at KRISS

Precision measurements of the quantum Hall plateau value in transported graphene devices have been performed. Comparison of precision measurements with different institutions is of importance for metrological applications. Compared to GaAs-based quantum Hall devices, graphene devices are less stable with respect to time or environment. This is a big challenge to be resolved. Thus, this becomes an obstacle for comparison measurements through transportation of graphene devices.

Precision measurements at KRISS have been performed with an epitaxial graphene device fabricated and pre-characterised by Aalto University and MIKES/VTI in Finland, respectively. Due to a change of doping level with time and environmental factors, doping level of the device had in each case to be readjusted with a combination of the photochemical doping, heating, and NH_3 treatment. For precision measurements at KRISS the square resistance was tuned to around 10 k Ω . The estimated combined uncertainty of measurements of R_H ($\nu=2$) against a 100 Ω resistor, calibrated by a GaAs quantum Hall device, is about 6 parts in 10^9 with a cryogenic current comparator resistance bridge in KRISS.

A relative deviation from the expected R_H ($\nu = 2$) of less than 30 parts in 10^9 was obtained down to 7 T of magnetic field and up to 6 K of temperature with a driving current of 19.37 μA . The observed deviation is consistent with previous precision measurements of the device in BIPM and MIKES/VTI. By the collaboration between KRISS and European institutes, KRISS was able to compare precision measurement results based on graphene quantum Hall devices even though they did not have suitable devices available made from their own hBN-graphene, due to the extreme challenges of producing QHR devices from this complex sandwiched material.

3.4 Assessment of the potential of graphene for impedance metrology

The use of a quantised Hall resistor at ac

PTB has carried out comprehensive measurements of the capacitance between a graphene Hall bar and surrounding conductive objects, which were either a back-gate, a side-gate, or a metal double-shield. Also the associated dissipation factors have been measured, worldwide for the very first time. These measurements provided the input information for modelling the frequency dependence of a graphene-based quantum Hall resistance. The model gives excellent agreement with the measured frequency dependence, which in turn shows that the reason of the frequency dependence is fully understood. In addition, the measurements gave new insight into the dissipation mechanism of graphene, in particular the role of the contacts. A publication on this topic is in preparation.

Upper limit of frequency dependence of R_{xy} at 1 Hz

Before this project started, it had been a concern that the frequency dependence of a graphene device might be very large and could even affect a quasi-dc measurement at a frequency as low as 1 Hz. This would limit the precision of the room-temperature current comparator operating developed in the project thread addressing '*Bespoke instrumentation for a simplified use*'. But in fact, it turned out that already for an unshielded graphene device without any ac-specific design the frequency dependence in the kHz range is always approximately linear (see Fig. 30) with a rate well below $1 \cdot 10^{-6} \text{ kHz}^{-1}$. Because the extrapolation of the ac quantum Hall resistance to zero hertz yields a value which is practically equal to the result of a dc measurement by a cryogenic current comparator, it is very unlikely that the frequency rate at low frequencies could be much higher. Therefore, the deviation of the 1 Hz value from the dc value will be well below $1 \cdot 10^{-9}$, which in turn is below the resolution of a room-temperature current comparator and therefore of no concern.

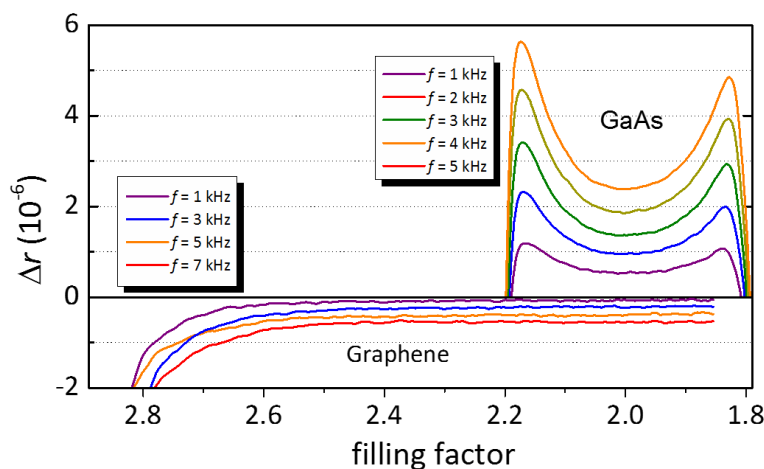


Fig. 30. Comparison of the QHR frequency dependence of bare (i.e. unshielded) GaAs and graphene devices. While GaAs exhibits a broad, curved plateau with positive frequency dependence, graphene shows a negative much smaller frequency dependence, flat over the very broad plateau. For easier comparison both groups of curves are plotted versus the filling factor instead of magnetic field.

Design guidelines for optimised ac-QHE graphene devices

As mentioned above, the measurements of the capacitance and the associated dissipation factor also involved the contribution of the contacts which are found to be essential for minimising the frequency dependence of an unshielded graphene device. Two approaches are conceivable:

- Firstly, while the geometry of a graphene device can be optimised to reduce the frequency dependence, it is not possible to null this dependence in a wider range of frequency and current. Thus, it is difficult to create a general guideline. However, as was shown by METAS, the method of extrapolating the frequency dependence to zero ac dissipation also works successfully with graphene devices of different design.
- The second approach is the double-shielding technique discussed below. Apart from the requirement that the middle potential contacts have to be smaller than the gap of the double-shield, and that the graphene Hall bar itself has to be much larger than the gap, the double-shielding approach does not cause any other ac-specific restriction of the device geometry.

Altogether, this means that the size and distance of the contacts is important, but major restrictions to the general layout do not exist.

Double-shielded ac-QHE devices

PTB has carried out ac measurements of the quantum Hall and longitudinal resistance of a graphene device mounted into a double-shield. Originally, the double-shielding technique had been developed at PTB for eliminating the unwanted frequency dependence of GaAs-based quantum Hall devices. Now we found that the double-shielding technique also successfully works with a graphene device and fully eliminates the unwanted frequency dependence within a relative uncertainty of $1.5 \cdot 10^{-9} \text{ kHz}^{-1}$. This is an absolutely great result. Provided that the future will enable a higher yield of graphene devices which are accurately quantised and withstand multiple temperature cycles, the way for a highly accurate graphene-based quantum impedance standard is paved now. The accuracy of the capacitance unit derived from such a graphene device would be as low as for the best GaAs devices (i.e., much better than for all available calculable capacitance artefacts), but it has the potential to be applied under the relaxed conditions (i.e., at higher temperatures and lower magnetic fields) offered by graphene. A publication on this topic is under way.

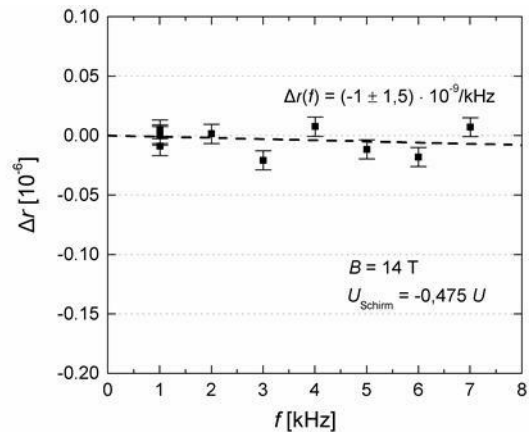
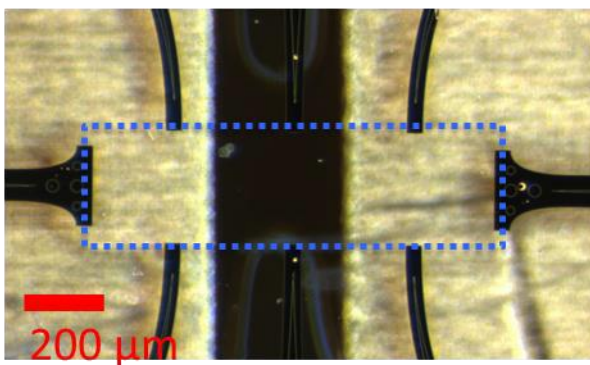


Fig. 31. Left: A $200 \times 800 \mu\text{m}^2$ graphene devices (dotted blue line) mounted above the lower half of a double shield (gold planes). Right: the residual frequency dependence of this devices is virtually zero, as it contributes at 1 kHz only $1.5 \cdot 10^{-9}$ to the measurement uncertainty.

Comparison of the double shield and extrapolation methods

ac measurements of R_{xy} and R_{xx} in graphene samples at frequencies up to 10 kHz were performed both at METAS and at PTB, on a batch of six graphene devices, all fabricated at PTB, from monolayer graphene films grown on the silicon-terminated face of a 6H silicon carbide substrate. At METAS a dedicated fully automated ac bridge was developed to perform measurements of the ac QHR, as described in [8,9,10]. The data obtained on the ac measurements of the QHR in both laboratories were grouped and analysed all together. This resulted in a much more consistent and clear view of the present status of the ac-QHE in graphene. The joint results, which are state of the art, have been submitted to IEEE [11] and were presented as a talk at CPEM 2016 [12]. They are summarised in the following paragraphs.

The frequency dependent deviation of the QHR from the nominal dc value $R_H = R_K/2$ is displayed in Fig. 32 for all samples. $\Delta R_H/R_H$ extrapolates close to zero at $f = 0$ which is compatible with the low dc R_{xx} values observed. The frequency dependence of ΔR_H is close to linear with the exception of sample G202. The slope of ΔR_H shows a large variation among the devices. All samples exhibit a negative slope except sample G202. Device G195B exhibits the smallest frequency dependence of the QHR with a slope of (-9 ± 3) ppb/kHz, smaller than observed in typical, unshielded GaAs devices.

ac longitudinal resistances R_{xx} as a function of frequency f are displayed in Fig. 33 for samples G195B, G195C, and G202. A positive linear frequency dependence of R_{xx} can be observed in samples G195C and G202. The small negative frequency dependence of R_{xx} for G195B is not significant, as the uncertainty of the slope of the linear fit is larger than the slope itself. The extrapolation to $f = 0$ is compatible with zero dissipation within the measurement uncertainty.

Measurement of both ac R_{xx} and ac R_{xy} as a function of f allows relating the deviation ΔR_H of the ac QHR from $R_K/2$ to the level of ac dissipation which is measured by the ac longitudinal resistivity $\rho_{xx} = (W/D) R_{xx}$, where W is the width of the channel and D the distance between the voltage probes. This relation is plotted in Fig. 34 for G195C in both the original and the reversed current configuration together with the weighted

linear fits. Since both ac ρ_{xx} and ac R_{xy} are very small for all measured frequencies in device G195B in comparison to G195C, the average ρ_{xx} was plotted against the average R_{xy} over all measured frequencies. Extrapolating ΔR_H (ρ_{xx}) to zero ac dissipation ($\rho_{xx} \rightarrow 0$) shows deviations of the extrapolated ac QHR from $R_H/2$ on the order of 5×10^{-8} . The linear dependence of the deviation and the extrapolation to zero dissipation is fully compatible with the observations made in semiconductor heterostructure based 2DEGs.

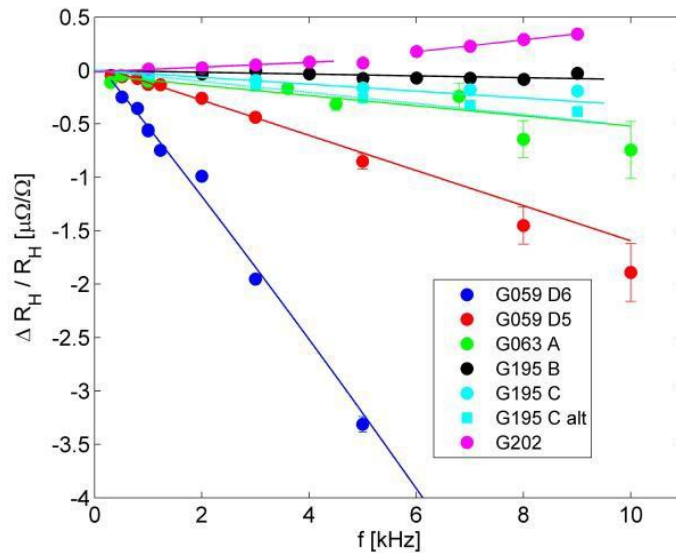


Fig. 32. Frequency dependence of the QHR measured in six different graphene samples up to 10 kHz.

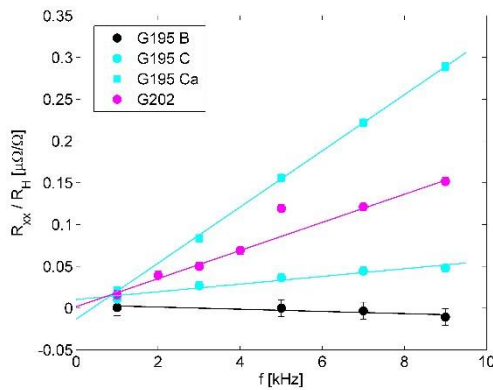


Fig. 33. AC R_{xx} as a function of frequency at $I = 10 \mu A$ for samples G202, G195B, and G195C.

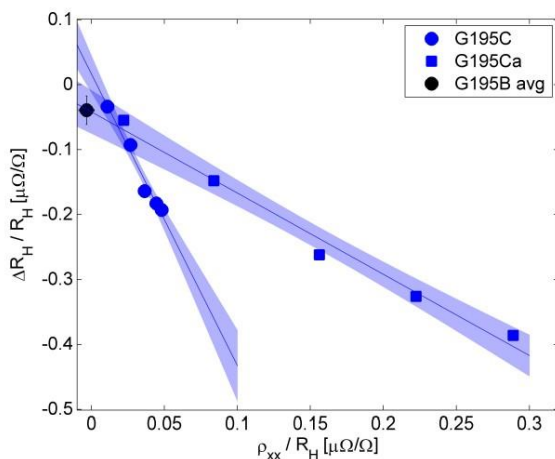


Fig. 34. Dependence of the deviation of the ac QHR from its nominal dc value as a function of ac dissipation for sample G195C in both original (G195C) and reversed (G195Ca) current configuration. Shaded surfaces represent 95% confidence intervals of the corresponding linear fits.

To summarise, a close to linear, negative frequency dependence of the ac QHR has been observed with considerable differences between individual samples. In one of our samples, the ac QHR only increased by less than one part in 10^7 from 0 to 10 kHz, which demonstrates the potential of the ac QHE in epitaxial graphene to realise a primary standard of impedance. The wide $\nu = 2$ plateau shown at dc is preserved at ac with a flatness which depends on the level of ac dissipation. Relating R_H to R_{xx} at ac reveals a linear relationship with a negative slope for a typical epitaxial graphene device. However, the extrapolation to zero dissipation shows a very good agreement with $R_K/2$, in full agreement with previous measurements in GaAs devices. In addition, one sample has shown an almost negligible frequency dependence both in R_{xy} and R_{xx} . A sample with vanishing ac dissipation represents the ideal candidate to realise a new graphene impedance standard where the ac resistance can be measured without any additional active shielding or further extrapolation method. The low ac dissipation demonstrated in this particular sample already allows for a realisation of the ac QHR at a precision level sufficient for most applications.

Finally, measurements with two dedicated devices having a particular geometry confirm the understanding of capacitive losses affecting the ac QHE. The positive and negative contributions to the measured ac R_{xy} depend on the device geometry. This geometrical dependence opens the way to design graphene Hall bars with vanishing dependence of ac R_{xy} on ac dissipation thus making the extrapolation procedure obsolete. In particular, in the asymmetric device G195C, the dependence of the capacitive losses on the current direction is a convincing demonstration of the dependence of the capacitive losses on the device dimensions.

3.5 Development of bespoke instrumentation for a simplified use of graphene

3.5.1 *Cryo-cooling in Graphene Metrology*

A cryo-cooled setup for realisation of the QHR without the need of external liquid helium supply has been developed within the project at CMI. It can be used for establishing measurement infrastructure for a widespread use of quantum standards in national metrology institutes, calibration laboratories, and at precision equipment manufacturer sites. At the beginning of the project, many cryo-cooled cryostats from different vendors were available, but heat load effects, mechanical vibrations, electromagnetic noise and absence of sample probe were limiting factors for realisation of QHR.

In the first step, a modular system based on a commercial liquid helium free magnet and a custom made cryo-cooled vacuum vessel was designed and assembled. With such a system, the first evaluation of graphene device behaviour in an environment cooled by a cryo-cooler with still rather high levels of mechanical vibration and electromagnetic noise was performed and the limitations of such cryo-coolers were assessed. Based on the acquired data, a proposal for the second system based on a commercially available cryo-cooled cryostat with integrated superconductive magnet was conceived. The system is based on re-condensation of a small amount of a helium gas. It does not need any liquid helium for the initial cool down. The system is able to operate nearly independent of outer sources of gases for several months due to the internal recuperation system. To achieve sufficiently high electrical and noise isolation properties of wirings, a special sample probe with a coaxial wiring between a break-out box and a low temperature stage with heat shields was fabricated with modifications for operation in cryogen-free cryostats. An improved fixation of the QHR sample position and its wiring against magnet fields was applied to suppress an effect of system vibration on measurement noise. The noise performance of the system was measured with a help of a room temperature operated current comparator during realisation of the QHR. Finally, project partners together with a collaborator have demonstrated the possibility of using the QHE to reproduce the unit of electrical resistance with an uncertainty below a few parts in 10^8 . This was shown outside of an NMI and without an external supply of liquid helium.



Fig. 35 A cryo-system, independent of external liquid Helium supply, with measurement equipment employed outside an NMI.

3.5.2 *Precision Low Frequency Room Temperature Current Comparator*

A precision resistance scaling device (Room Temperature Current Comparator, RTCC) has been developed and tested in resistance ratio measurements with a graphene QHR at ultra-low frequency. The device can substitute the more expensive scaling instrument (Cryogenic Current Comparator, CCC), which needs liquid helium for its operation. Yet the RTCC keeps the uncertainty of the scaling at a sufficiently low value. When used in a QHR setup, the RTCC significantly reduces the investment, as well as the cost of operation of the whole resistance calibration setup.

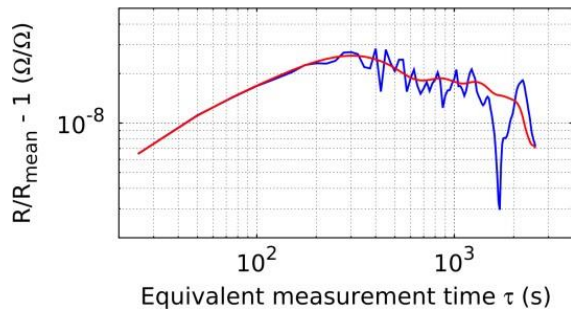


Fig. 36 Allan deviation (blue) and overlapped Allan deviation (red) of measured ratio $R_k/2 \approx 12.9 \text{ k}\Omega$ and $1 \text{ k}\Omega$ artefact.

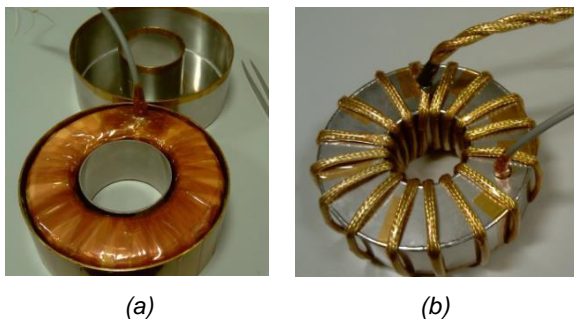


Fig. 37. RTCC made at MIKES. The panels display photographs of RTCC taken during manufacturing: Panel (a) shows magnetic core and detection coil after inclusion into an isolated electrostatic shield and wrapping with insulating Kapton® foil. This torus is inserted into one part of the magnetic shield consisting of two half-shells made of μ -metal. Panel (b) shows the not yet finished comparator with one cable containing ratio windings which is wound 16 times around the magnetic shield.

At present, in most leading NMIs, a CCC is used as precision scaling device for resistance ratio measurements. Application of a CCC requires low (liquid helium) temperatures, its operation is very complex and the used devices are very sensitive to external interference. An alternative to a CCC is an RTCC, which provides accurate reference ratios by operating at a low frequency. A prototype of such an RTCC had been developed at BIPM, showing unique properties for the measurement of resistance ratios with a combined uncertainty at the level of few parts in 10^9 . It operates, however, only at 1 Hz and requires correction for evaluation of the “dc” value of resistors. The challenge in this project was to achieve operation at a still lower measurement frequency (in the SI the quantity resistance is defined at 0 Hz). The new instrument offers simplicity of operation, transportability, and on-demand operability, thus disposing of the need for expensive liquid helium, or helium refrigerators and liquid helium facilities.

For accurate resistance ratio measurement and in particular for the ratio of the QHR to the decimal values of secondary resistance standards two prototypes of a high sensitivity ultra-low frequency RTCC have been developed. In order to extend the frequency range close to zero frequency, we have chosen and used high permeability magnetic cores (based on amorphous magnetic alloys), have fabricated a high inductance detection coil, and improved the design of electrostatic and magnetic shields. The combination of these actions allowed to increase the sensitivity of the RTCC even at very low frequencies providing the desired level of uncertainty. The sets of numbers of turns chosen for the ratio windings enable to use RTCCs with ratios of 100:1, 10:1, 1:1, and for the QHR-to-100 Ω ratio of about 129:1 when choosing an effective numbers-of-turns ratio of 2065:16. In Fig. 37 photographs of the RTCC setup taken during its manufacturing are presented. The RTCC developed in this project has achieved a sensitivity at significantly low (0.15 Hz) frequency, which was never reached, allowing to reach a low measurement uncertainty at the level of parts in 10^9 . The RTCC combines the simplicity of room temperature operation with a precision not attainable with commercial room temperature equipment before, approaching that of Helium-operated cryogenic current comparators. The new RTCC can be used not only in newly established calibration systems, but it can also be retrofitted into existing systems, replacing cryogenic current comparators (CCC).

3.6 Summary of the key results and conclusions

To summarise, the key results of this project are as follows:

The *Development and advancement of graphene and graphene device fabrication* objective has been achieved by advancing the growth technique of graphene on SiC considerably. Besides increasing the capability for SiC-G growth from small 10x10 mm² pieces to full-wafer-growth, the methods to minimise the growth of the detrimental bilayer graphene have also been advanced. It is now possible to grow graphene reliably and with excellent yield, avoiding or minimising the limitations previously encountered with graphene as a material for resistance standards. Further, the number of institutes able to grow the kind of graphene which is usable for a precision QHE application has been increased since now also Chalmers, PTB, and a cooperating CNRS institute are capable of growing SiC-G.

The *Development of better characterisation methods* objective has been achieved by developing or refining and successfully applying various scanning probe microscopy methods, a non-destructive and quick microwave characterisation method, the Raman method, and the liquid crystal texture method. In summary, more accurate, quantitative, non-destructive characterisation procedures were developed which not only have enabled progress in the graphene film fabrication within the project, but are valuable for the emerging graphene industry well beyond the project.

The *Exploration of the limits of graphene in precision resistance metrology* objective has been achieved by developing methods for the tuning of the carrier density of devices to such a low level that they can be used at those low magnetic fields where their inherent advantage over the traditional material GaAs can be fully exploited. Based on these methods it was possible to demonstrate the superior performance of graphene at a combination of magnetic field, temperature, and measurement current which enables the use of this quantum standard outside NMIs. An increased and better understanding of the physical mechanisms which might compromise the attainable precision upon approaching extremes of the field, temperature, and current ranges has been achieved and is the basis of the reliance on graphene QHE quantum standards that users can have now.

The *Assessment of the potential of graphene for impedance metrology* objective has been achieved by demonstrating that mechanisms leading to dielectric losses in the kHz range, where impedance standards are typically used, play no significant role. The most convincing proof of this is a virtually vanishing frequency dependence of the graphene quantised Hall resistance. The route to extend graphene's use as a quantum standard of resistance also to the ac realm of impedance is now fully open.

Last but not least, the *Development of bespoke instrumentation for a simplified use of graphene resistance standards* objective has been achieved by developing, fabricating, and extensively testing and verifying a resistance ratio bridge. It can match the uncertainty of the cryogenic current comparator instruments but can be used simply at room temperature, not requiring liquid Helium for its operation. Also the development of closed cycle coolers and the demonstration of their application with graphene resistance standards was achieved in this part of the project.

In conclusion, all objectives of the project have been achieved. Even those parts where an outcome was negative, like the attempts to make and use graphene grown with the CVD method for precision measurements, have been very valuable, since the reasons for this failure (of at least the current generation of CVD-graphene) have been investigated and could be understood. This, and the mere fact that discovering this at an early stage allowed concentrating the resources on more promising routes, has been an advantage. What remains to be done for the future is the attempt to simplify the carrier tuning procedures, or to find adapted growth regimes which yield a lower carrier density just by the growth, removing the requirement of the carrier tuning methods altogether.

4 Actual and potential impact

4.1 Metrology achievements

The technology of graphene based resistance standards has been called 'potentially disruptive' since the projected leap from the complex-to-operate GaAs based quantum resistance, to a closed-cycle cooler, small magnet environment is really that: disruptive.

The availability of the best imaginable standard of resistance, the fundamental constant based QHE reference, will significantly improve calibrations of the important quantity resistance by shortening the calibration chains, making them more efficient and economic. A standard that is more widely distributed, with the primary reference available wherever it is needed, will reduce the costs, complexity and inconveniences of traditional approaches. Such improved dissemination will constitute a real breakthrough not only for calibration laboratories, but also for those NMIs which up to now have not been able to afford to operate the complex quantum standards. These NMIs are often in an even worse situation than an industrial calibration laboratory with high throughput. While the latter are typically located in a country with excellent and easily accessible NMI infrastructure, the metrology capacity of those Member States (and countries associated with the Seventh Framework Programme) whose metrology programmes are at an early stage of development face severe logistic and financial problems to maintain the traceability of their national standards. The widely available and simplified quantum standard of resistance which can now be implemented is improving this situation significantly.

The key achievements of this project are new, simpler to operate quantum resistance standards and adapted instrumentation to exploit them. These intrinsically referenced resistance standards, based on a new and remarkable electronic material, graphene, have a ground-breaking effect on the metrology landscape. It will enable the dissemination of quantum based electrical units in a simpler and quicker way than ever before.

The graphene based QHR standard is being used in a number of metrology labs already, among them NPL, RISE, PTB, MIKES, and, outside Europe, the U.S.-based NIST.

Beyond that, at PTB, and very likely in the near future also at METAS and CMI, the use of graphene as an impedance standard is being very seriously considered: the additional requirements of an ac-application make graphene even more ideal due to its additional advantages over GaAs at ac (besides the lower field and higher temperature operability).

In summary, three key developments within the project are producing direct impact:

- Graphene-based quantum Hall effect devices operating under strongly relaxed conditions of temperature and magnetic field, along with a technological method of fabricating them, significantly increase the user base of ultimately precise intrinsically referenced standards.
- The specific instrumentation to utilise the graphene QHE devices, differing from instrumentation exploiting traditional GaAs-devices in terms of simplicity and added capability for device conditioning is available, together with simplified but vital accessory instrumentation.
- The project objective on the use of the QHE at ac frequencies has provided the key foundations for the wider use of QHE devices also as a standard of impedance. The design guidelines for ac-optimised devices, for double shielded ac-QHE devices, and details about the measurement procedures have been published and are available to interested parties.

Collaborators and stakeholders, representing the worldwide NMI community, industrial calibration labs, and special equipment manufacturers have been involved in a stakeholder committee consulting closely with the project Consortium in order to ensure timely exchange of relevant information.

The following two patent applications have been filed:

- Procedure for producing Graphene (filed by PTB, granted as European patent EP 3 106 432 A1)
- Single crystalline gCVD-graphene growth (filed by KRISS)

4.2 Examples of early impact

A strong early impact has been achieved by the involvement of the *Bureau International des Poids et Mesures*, *BIPM*. As the highest international authority in the worldwide measurement system, BIPM was the ideal partner to achieve a maximum lever arm effect for the results of this project.

This is reflected in

- the [News article of the CCEM](#) (Consultative Committee for Electricity and Magnetism): with direct reference to the GraphOhm outcome, the article states that “Significant progress on the quantum Hall effect with graphene samples ... will lead to simpler and lower cost quantum resistance standards, and in consequence to their wider use.”
- the [News article of BIPM](#) where the collaboration between BIPM and the project is mentioned again. The article says that “In the ... GraphOhm EURAMET project, samples developed in a collaboration ... proved suitable for calibration ... (BIPM) envisage(s) being able to implement a much simplified transportable system The collaboration ... also involved the investigation of a new generation of (instrumentation) ... that could ... accompany the new graphene reference.”

The proliferation of the technology to NMIs which were not partners of GraphOhm (or have large enough resources that they could progress on their own, like NIST has) is also progressing. Project partner RISE has clearly shown that by just retrofitting an existing calibration system with graphene devices, smaller NMIs will see immediate improvements, both in terms of accuracy and operating costs. This constitutes an early potential impact for all laboratories which currently operate QHR systems.

Immediately after the project, Italian NMI INRIM has contacted project coordinator PTB and expressed their interest in further development of graphene devices. As an outcome of this discussion INRIM and PTB decided to jointly fund a PhD student at INRIM to be delegated to PTB in order to learn and assist in the fabrication of graphene QHR devices for both INRIM and PTB.

A future impact will be realised when companies who adapt or develop dedicated measurement setups will utilise the simplifications enabled by the project and deliver their products to customers. Right now the following examples can be given:

- UK based [Oxford Instruments plc](#) already brought to market a closed cycle cooler system adapted for graphene QHE measurements.
- Swedish based [GraphenSIC](#) is marketing graphene devices and a graphene QHR system
- Canada based [Measurement International \(MI\)](#), the world-leading manufacturer of instrumentation and systems for resistance metrology announced during the project’s final dissemination meeting that they will bring a graphene based quantum resistance standard to market in the near future.

4.3 Dissemination activities

4.3.1 Scientific publications

The project consortium has published 56 papers, some of them in high ranked journals like Nature, Carbon, Advanced Materials, etc. Approx. 50 of these papers were published under the open access policy, and may be accessed via the EURAMET publications repository or the project web page (see below).

4.3.2 Conferences and relevant fora

In addition, the work carried out in the project has been communicated to the wider scientific audience through nearly 100 contributions to general conferences such as the *APS* and *E-MRS Spring Meetings*, as well as to targeted audiences in specialised conferences such as the Conference on Precision Electromagnetic Measurements (Rio de Janeiro, BRA, 2014, and Ottawa, CAN, 2016) and the *Graphene Week* meetings 2014, ‘15, and ‘16.

In total, 54 oral presentations as well as 38 poster presentations have been given by the partners during the life time of the project. Positive reactions were received to all these contributions, attracting discussions and comments.

Presentations of the outcomes of the project have also been given at a number of key fora, in particular at EURAMET and BIPM-CCEM working groups' meetings, where it has resulted in the influence of future strategy ensuring on-going impact of the project into the future.

4.3.3 Workshops

Two stakeholder workshops have been organised during the lifetime of the project. During the first one, held in Teddington, UK in November 2014 in conjunction with the periodic meeting of the project and the *Graphene & 2-D Materials Conference 2014*, more than forty participants attended the meeting, including representatives from industry, from research laboratories and academic groups. During the conference, seven presentations of project results were given by consortium members. Also invited speakers presented their activities and their latest research results.

A dissemination workshop for GraphOhm (Joint workshop with two other EMRP projects with similar audience – SIB53 AIM QuTE and SIB59 Q-Wave) was held in Prague, 18-19 May 2016, with an audience of over 55 project partners and stakeholders. Summarising project talks focused on the project challenges, their solutions, and on the outcomes of the projects. During a poster session technical details and the impact of project outputs on the NMI and non-NMI communities were intensely discussed. The meeting was a place of very fruitful knowledge exchange between partners, stakeholders, and collaborators. Also the future needs of metrology were discussed.

Directly after the dissemination workshop, a live training course on the use of graphene as a QHE resistance standard was held. The training was focused on the topics most important for the user community, like preparation of devices, their conditioning and handling, and the optimal measurement instrument configuration.

4.4 Potential impact

The improved methods for characterising graphene films have already found their way into various laboratories where graphene films are grown for research or for applications, e.g. in the field of electronics.

The uptake of project outputs in the metrology community will lead to further environmental, social and financial impacts, although the exact route to this is extremely hard to quantify in detail due to the basic and general importance of the quantities 'electrical resistance' and 'impedance'. Measuring them precisely benefits strongly from bringing their quantum standard based realisation method to the end-user. However, since these quantities are at the root of an often very long and complex chain of measurements, these beneficial effects are hard to visualise.

Nevertheless, the following statements about the anticipated indirect impact can be made:

- The high-yield method for growth of large-area graphene wafers with high uniformity and quality for a scalable and versatile graphene technology, as achieved in this project, is contributing to progress in a range of applications beyond the metrology field, e.g. in the area of sensor applications of graphene (sensitive gas sensors, Hall effect sensors for small magnetic fields, radiation sensors).
- The extended availability of a better and simpler resistance standard is giving an additional boost for the development of materials and devices with improved stability and accuracy for all technological fields where resistive properties of materials play a role, be it for temperature sensors, capacitive sensors for all kinds of non-electrical quantities, resistive read-heads, to name just a few.
- The redefinition of the kilogram will in the future 'New SI' be based on the Planck constant h . The connection to h in a so-called Kibble-balance requires use of the Josephson and Quantum Hall Effects, and therefore the simpler to use graphene-based resistance standard will have strong impact for those future primary mass standards, which operate at very low uncertainty..

4.5 Projected impact on EC Directives, and other relevant standards

The fundamental role of the electrical quantities, among them prominently the quantity resistance, in our measurement system is evident from the following documents:

- The Resolution¹ on the future revision of the International System of Units (SI), adopted by the General Conference on Weights and Measures (CGPM) at its 24th meeting (October 2011): This

Resolution takes note of the revision of the SI and sets out a detailed road-map towards the future changes. As a paradigmatic change in the new SI, base units of the SI will be defined by adopting fixed values for fundamental constants of nature, like h and e , whose simplified exploitation is the key achievement of this project.

- The future *mise en pratique*² for the ampere and other electric units, prepared by the Consultative Committee for Electricity and Magnetism (CCEM): In this document the role of the QHE for the units ohm (Ω), ampere (A), farad (F), and henry (H) is clearly stated.
- The importance of the QHE for the unit kilogram (kg) is based on the fact that a quantised Hall resistance in combination with a Josephson voltage can be used in an electromechanical balance to realise the Planck constant based mass unit. This is outlined in a *mise en pratique*³ prepared by the Consultative Committee for Mass (CCM).

Further, calibration is an important and recurring subject in the EC directive MID 2004/22/IEC on measuring instruments. National laws and Directives in the EU Member States concerning the units of measurements and how they are to be implemented⁴ will be impacted by simpler, better, and more cost-effective implementation of the metrology for resistance.

The following communication paths were used by project partners to prepare the project results' future impact on written standards:

- CCEM and its working groups: they advise the CIPM on matters related to electrical standards
- TC-EM (EURAMET) and its working groups: they discuss issues of more technical nature which are important to industry and researchers.

5 Website address and contact details

The address of the JRP website is:

<http://www.ptb.de/emrp/graphohm.html>.

A partners' restricted area has also been created, in order to give the possibility to all the partners to share work documents and deliverables: <http://www.ptb.de/emrp/sib51-members-bscw.html> (the password is available on request).

The contact person for general questions about the project is

Dr Franz Josef Ahlers
 Physikalisch-Technische Bundesanstalt
 Bundesallee 100
 DE-38116 Braunschweig, Germany

Phone: +49 531 592 2610

Email: franz.ahlers@ptb.de)

¹ http://www.bipm.org/utis/en/pdf/24_CGPM_Resolution_1.pdf

² <http://www.bipm.org/cc/CCEM/Allowed/26/CCEM-09-05.pdf>

³ http://www.bipm.org/cc/CCM/Allowed/15/02A_MeP_kg_141022_v-9.0_clean.pdf

⁴ E.g., in Germany the "[Law on Measuring Units and Time \(EinhZeitG\)](#)"

6 List of publications

- [1] Wang, R., Pearce, R., Gallop, J., Patel, T., Zhao, F., Pollard, A., ... Hao, L. (2016). Investigation of CVD graphene topography and surface electrical properties. *Surface Topography: Metrology and Properties*, 4(2), 25001. <https://doi.org/10.1088/2051-672X/4/2/025001>
- [2] Hao, L., Gallop, J., Chen, J., Adabi, M., Klein, N., Sierakowski, A., ... Gotszalk, T. (2015). Self-supporting graphene films and their applications. *IET Circuits, Devices & Systems*, 9(6), 420–427. <https://doi.org/10.1049/iet-cds.2015.0149>
- [3] Pearce, R., Tan, X., Wang, R., Patel, T., Gallop, J., Pollard, A., ... Hao, L. (2014). Investigations of the effect of SiC growth face on graphene thickness uniformity and electronic properties. *Surface Topography: Metrology and Properties*, 3(1), 15001. <https://doi.org/10.1088/2051-672X/3/1/015001>
- [4] Hill Pearce, R. E., Eless, V., Lartsev, A., Martin, N. A. A., Barker Snook, I. L. L., Helmore, J. J. J., ... Hao, L. (2015). The effect of bilayer regions on the response of epitaxial graphene devices to environmental gating. *Carbon*, 93, 896–902. [article. https://doi.org/10.1016/j.carbon.2015.05.061](https://doi.org/10.1016/j.carbon.2015.05.061)
- [5] Lafont, F., Ribeiro-Palau, R., Han, Z., Cresti, A., Delvallée, A., Cummings, A. W., ... Poirier, W. (2014). Anomalous dissipation mechanism and Hall quantisation limit in polycrystalline graphene grown by chemical vapor deposition. *Physical Review B*, 90(11), 115422. <https://doi.org/10.1103/PhysRevB.90.115422>
- [6] Lafont, F., Ribeiro-Palau, R., Kazazis, D., Michon, A., Couturaud, O., Consejo, C., ... Poirier, W. (2015). Quantum Hall resistance standards from graphene grown by chemical vapour deposition on silicon carbide. *Nature Communications*, 6, 6806. <https://doi.org/10.1038/ncomms7806>
- [7] Ribeiro-Palau, R., Lafont, F., Brun-Picard, J., Kazazis, D., Michon, A., Cheynis, F., ... Schopfer, F. (2015). Quantum Hall resistance standard in graphene devices under relaxed experimental conditions. *Nature Nanotechnology*, 10(11), 965–971. <https://doi.org/10.1038/nnano.2015.192>
- [8] F. Overney, F. Lüönd and B. Jeanneret, Digitally Assisted Coaxial Bridge for Automatic Quantum Hall Effect Measurements at Audio Frequencies, Proceedings of the Conference on Precision Electromagnetic Measurements, pp. 226-227, 2014.
- [9] F. Overney, Digitally Assisted Coaxial Bridge for Automatic Quantum Hall Effect Measurements at Audio Frequencies, Talk presented at the Conference on Precision Electromagnetic Measurements, Rio de Janeiro, August 2014.
- [10] F. Overney, F. Lüönd and B. Jeanneret, Broadband Fully Automated Digitally Assisted Coaxial Bridge for High Accuracy Impedance Ratio Measurements, *Metrologia* 53, pp. 918–926, 2016.
- [11] F. Lüönd, C. C. Kalmbach, F. Overney, J. Schurr, B. Jeanneret, A. Müller, M. Kruskopf, K. Pierz and F.-J. Ahlers, AC Quantum Hall Effect in Epitaxial Graphene, submitted to *IEEE Trans. Instrum. Meas.*, 2016.
- [12] F. Lüönd, AC Quantum Hall Effect in Epitaxial Graphene, Talk presented at the Conference on Precision Electromagnetic Measurements, Ottawa, July 2016.
- [13] Chen, J., Liu, Q., Gallop, J., & Hao, L. (2015). Microwave method for high-frequency properties of graphene. *IET Circuits, Devices & Systems*, 9(6), 397–402. <https://doi.org/10.1049/iet-cds.2015.0114>
- [14] Woszczyzna, M., Winter, A., Grothe, M., Willunat, A., Wundrack, S., Stosch, R., ... Turchanin, A. (2014). All-Carbon Vertical van der Waals Heterostructures: Non-destructive Functionalisation of Graphene for Electronic Applications. *Advanced Materials*, 26(28), 4831–4837. <https://doi.org/10.1002/adma.201400948>
- [15] Novikov, S., Lebedeva, N., & Satrapinski, A. (2014). Fabrication and study of large area QHE devices based on epitaxial graphene. In *29th Conference on Precision Electromagnetic Measurements (CPEM 2014)* (pp. 32–33). IEEE. <https://doi.org/10.1109/CPEM.2014.6898244>
- [16] Lartsev, A., Lara-Avila, S., Danilov, A., Kubatkin, S., Tzalenchuk, A., & Yakimova, R. (2015). A prototype of RK/200 quantum Hall array resistance standard on epitaxial graphene. *Journal of Applied Physics*, 118(4), 44506. <https://doi.org/10.1063/1.4927618>
- [17] Panchal, V., Giusca, C. E., Lartsev, A., Yakimova, R., & Kazakova, O. (2014). Local electric field screening in bi-layer graphene devices. *Frontiers in Physics*, 2, 3.

- <https://doi.org/10.3389/fphy.2014.00003>
- [18] Ahlers, F., Kucera, J., Poirier, W., Jeanneret, B., Satrapinski, A., Tzalenchuk, A., ... Kubatkin, S. (2014). The EMRP project GraphOhm - Towards quantum resistance metrology based on graphene. In *29th Conference on Precision Electromagnetic Measurements (CPEM 2014)* (pp. 548–549). IEEE. <https://doi.org/10.1109/CPEM.2014.6898502>
- [19] Kalmbach, C.-C., Schurr, J., Ahlers, F. J., Müller, A., Novikov, S., Lebedeva, N., & Satrapinski, A. (2014). Towards a graphene-based quantum impedance standard. *Applied Physics Letters*, *105*(7), 73511. article. <https://doi.org/10.1063/1.4893940>
- [20] Yager, T., Webb, M. J., Grennberg, H., Yakimova, R., Lara-Avila, S., & Kubatkin, S. (2015). High mobility epitaxial graphene devices via aqueous-ozone processing. *Applied Physics Letters*, *106*(6), 63503. <https://doi.org/10.1063/1.4907947>
- [21] Kim, D. H., Kim, S.-J., Yu, J.-S., & Kim, J.-H. (2015). Measuring the Thickness of Flakes of Hexagonal Boron Nitride Using the Change in Zero-Contrast Wavelength of Optical Contrast. *Journal of the Optical Society of Korea*, *19*(5), 503–507. <https://doi.org/10.3807/JOSK.2015.19.5.503>
- [22] Chua, C., Connolly, M., Lartsev, A., Yager, T., Lara-Avila, S., Kubatkin, S., ... Smith, C. G. (2014). Quantum Hall Effect and Quantum Point Contact in Bilayer-Patched Epitaxial Graphene. *Nano Letters*, *14*(6), 3369–3373. <https://doi.org/10.1021/nl5008757>
- [23] Satrapinski, A., Novikov, S., & Lebedeva, N. (2013). Precision Quantum Hall Resistance Measurement on Epitaxial Graphene Device in Low Magnetic Field. *Applied Physics Letters*, *103*(173509) (2013). article. <https://doi.org/10.1063/1.4826641>
- [24] Kruskopf, M., Pierz, K., Wundrack, S., Stosch, R., Dziomba, T., Kalmbach, C.-C. C., ... Tegenkamp, C. (2015). Epitaxial graphene on SiC: Modification of structural and electron transport properties by substrate pretreatment. *Journal of Physics: Condensed Matter*, *27*(18), 185303. article. <https://doi.org/10.1088/0953-8984/27/18/185303>
- [25] Lara-Avila, S., Kubatkin, S., Kashuba, O., Folk, J. A., L'vov, S., Yakimova, R., ... Fal'ko, V. (2015). Influence of Impurity Spin Dynamics on Quantum Transport in Epitaxial Graphene. *Physical Review Letters*, *115*(10), 1–5. <https://doi.org/10.1103/PhysRevLett.115.106602>
- [26] Thodkar, K., Nef, C., Fu, W., Schönenberger, C., Calame, M., Lüönd, F., ... Jeanneret, B. (2014). CVD Graphene for Electrical Quantum Metrology. In *29th Conference on Precision Electromagnetic Measurements (CPEM 2014)* (pp. 540–541). proceedings, IEEE. <https://doi.org/10.1109/CPEM.2014.6898498>
- [27] Janssen, T. J. B. M., Giusca, C., Gallop, J., Hao, L., Kazakova, O., Panchal, V., ... Tzalenchuk, A. (2014). Graphene metrology. In *29th Conference on Precision Electromagnetic Measurements (CPEM 2014)* (pp. 662–663). proceedings, IEEE. <https://doi.org/10.1109/CPEM.2014.6898559>
- [28] Schurr, J., Ahlers, F., & Pierz, K. (2014). Magnetocapacitance and loss factor of GaAs quantum Hall effect devices. *Metrologia*, *51*(3), 235–242. <https://doi.org/10.1088/0026-1394/51/3/235>
- [29] Lafont, F., Ribeiro-Palau, R., Cresti, A., Han, Z., Cummings, A. W., Roche, S., ... Poirier, W. (2014). Dissipative quantum Hall effect in polycrystalline CVD graphene. In *29th Conference on Precision Electromagnetic Measurements (CPEM 2014)* (pp. 42–43). proceedings, IEEE. <https://doi.org/10.1109/CPEM.2014.6898249>
- [30] Janssen, T. J. B. M., Rozhko, S., Tzalenchuk, A., Alexander-Webber, J. A., & Nicholas, R. J. (2014). Breakdown of the quantum Hall effect in epitaxial graphene. In *Breakdown of the quantum Hall effect in epitaxial graphene* (pp. 40–41). proceedings, IEEE. <https://doi.org/10.1109/CPEM.2014.6898248>
- [31] Overney, F., Luond, F., Jeanneret, B., Lüönd, F., & Jeanneret, B. (2014). Digitally assisted coaxial bridge for automatic quantum Hall effect measurements at audio frequencies. In *29th Conference on Precision Electromagnetic Measurements (CPEM 2014)* (pp. 226–227). proceedings, IEEE. <https://doi.org/10.1109/CPEM.2014.6898341>
- [32] Robinson, B. J., Giusca, C. E., Gonzalez, Y. T., Kay, N. D., Kazakova, O., & Kolosov, O. V. (2015). Structural, optical and electrostatic properties of single and fewlayers MoS₂: effect of substrate. *Structural, Optical and Electrostatic Properties of Single and Fewlayers MoS₂: Effect of Substrate*, *2*(1), 15005. article. <https://doi.org/10.1088/2053-1583/2/1/015005>
- [33] Janssen, T. J. B. M. J. B. M., Rozhko, S., Antonov, I., Tzalenchuk, A., Williams, J. M., Melhem, Z., ...

- Yakimova, R. (2015). Operation of graphene quantum Hall resistance standard in a cryogen-free table-top system. *Operation of Graphene Quantum Hall Resistance Standard in a Cryogen-Free Table-Top System*, 2(3), 35015. article. <https://doi.org/10.1088/2053-1583/2/3/035015>
- [34] Panchal, V., Lartsev, A., Manzin, A., Yakimova, R., Tzalenchu, A., Kazakova, O., ... Kazakova, O. (2014). Visualisation of edge effects in side-gated graphene nanodevices. *SCIENTIFIC REPORTS*, 4: 5881, 5881. article. <https://doi.org/10.1038/srep05881>
- [35] Huang, J., Alexander-Webber, J. A., Baker, A. M. R., Janssen, T. J. B. M., Tzalenchuk, A., Antonov, V., ... Nicholas, R. J. (2015). Disorder induced Dirac-point physics in epitaxial graphene from temperature-dependent magneto-transport measurements. *Disorder Induced Dirac-Point Physics in Epitaxial Graphene from Temperature-Dependent Magneto-Transport Measurements*. article. <https://doi.org/10.1103/PhysRevB.92.075407>
- [36] Yager, T., Lartsev, A., Cedergren, K., Yakimova, R., Panchal, V., Kazakova, O., ... Kubatkin, S. (2015). Low contact resistance in epitaxial graphene devices for quantum metrology. *AIP Advances*, 5(8), 87134. <https://doi.org/10.1063/1.4928653>
- [37] Yu, J.-S., Jin, X., Park, J., Kim, D. H., Ha, D.-H., Chae, D.-H., ... Kim, J.-H. (2014). Structural analysis of graphene synthesised by chemical vapor deposition on copper foil using nematic liquid crystal texture. *Carbon*, 76, 113–122. <https://doi.org/10.1016/j.carbon.2014.04.057>
- [38] Byun, I.-S., Kim, W., Boukhvalov, D. W., Hwang, I., Son, J. W., Oh, G., ... Park, B. H. (2014). Electrical control of nanoscale functionalisation in graphene by the scanning probe technique. *NPG Asia Materials* (2014) 6, 102(5), e102. article. <https://doi.org/10.1038/am.2014.24>
- [39] Huang, J., Alexander-Webber, J. A., Janssen, T. J. B. M. J. B. M., Tzalenchuk, A., Yager, T., Lara-Avila, S., ... Nicholas, R. J. (2014). Hot carrier relaxation of Dirac fermions in bilayer epitaxial graphene. *Journal of Physics: Condensed Matter*, 27(16), 164202. article. <https://doi.org/10.1088/0953-8984/27/16/164202>
- [40] Satrapinski, A., Pontynen, H., Gotz, M., Pesel, E., Fletcher, N., Goebel, R., ... Rolland, B. (2014). A Low-Frequency Current Comparator For Precision Resistance Measurements. In *A Low-Frequency Current Comparator For Precision Resistance Measurements* (pp. 760–761). proceedings, IEEE. <https://doi.org/10.1109/CPEM.2014.6898608>
- [41] Novikov, S., Lebedeva, N., Satrapinski, A., Novikov, S., Lebedeva, N., & Satrapinski, A. (2015). Ultrasensitive NO₂ Gas Sensor Based on Epitaxial Graphene. *Journal of Sensors*, 2015, 1–7. <https://doi.org/10.1155/2015/108581>
- [42] Alexander-Webber, J. A., Huang, J., Maude, D. K., Janssen, T. J. B. M., Tzalenchuk, A., Antonov, V., ... Nicholas, R. J. (2016). Giant quantum Hall plateaus generated by charge transfer in epitaxial graphene. *Scientific Reports*, 6(May), 30296. <https://doi.org/10.1038/srep30296>
- [43] Bergsten, T., & Eklund, G. (2016). Comparison Between GaAs and Graphene QHR Standards for Resistance Realisation at SP. In *Digest on Conference on Precision Electromagnetic Measurements (CPEM2016)*. proceedings, IEEE. <https://doi.org/10.1109/CPEM.2016.7540514>
- [44] Brun-Pcard, J., Ribeiro-Palau, R., Lafont, F., Kazazis, D., Michon, A., Cheynis, F., ... Schopfer, F. (2016). Convenient Graphene-Based Quantum Hall Resistance Standards. In *Digest on Conference on Precision Electromagnetic Measurements (CPEM2016)*. proceedings, IEEE. <https://doi.org/10.1109/CPEM.2016.7540650>
- [45] Chae, D.-H., Kim, W.-S., Satrapinski, A., & Novikov, S. (2016). Precision measurements of quantum hall resistance plateau in doping-controlled graphene device. In *2016 Conference on Precision Electromagnetic Measurements (CPEM 2016)* (pp. 1–2). IEEE. <https://doi.org/10.1109/CPEM.2016.7540495>
- [46] Dong Hyun, K., Sung-Jo, K., Jeong-Seon, Y., & Jong-Hyun, K. (2015). Measuring the Thickness of Flakes of Hexagonal Boron Nitride Using the Change in Zero-Contrast Wavelength of Optical Contrast. *Measuring the Thickness of Flakes of Hexagonal Boron Nitride Using the Change in Zero-Contrast Wavelength of Optical Contrast*, 19(5), 503–507. article. <https://doi.org/10.3807/JOSK.2015.19.5.503>
- [47] He, H., Janssen, T. J. B. M., Rozhko, S., Tzalenchuk, A., Lara-Avila, S., Yakimova, R., & Kubatkin, S. (2016). Fabrication of graphene quantum Hall resistance standard in a cryogen-free table-top system. In *Digest on Conference on Precision Electromagnetic Measurements (CPEM2016)*. proceedings, IEEE. <https://doi.org/10.1109/CPEM.2016.7540516>

- [48] Janssen, T. J. B. M., Giusca, C., Gallop, J., Hao, L., Kazakova, O., Panchal, V., ... Tzalenchuk, A. (2014). Graphene metrology. In *29th Conference on Precision Electromagnetic Measurements (CPEM 2014)* (pp. 662–663). proceedings, IEEE. <https://doi.org/10.1109/CPEM.2014.6898559>
- [49] Kalmbach, C.-C., Schurr, J., Muller, A., Kruskopf, M., Pierz, K., & Ahlers, F. J. (2016). Dissipation factor and frequency dependence of graphene quantum Hall devices. In *2016 Conference on Precision Electromagnetic Measurements (CPEM 2016)* (pp. 1–2). IEEE. <https://doi.org/10.1109/CPEM.2016.7540518>
- [50] Lartsev, A., Yager, T., Bergsten, T., Tzalenchuk, A., Janssen, T. J. B. M., Yakimova, R., ... Kubatkin, S. (2014). Tuning carrier density across Dirac point in epitaxial graphene on SiC by corona discharge. *Applied Physics Letters*, *105*(6), 63106. article. <https://doi.org/10.1063/1.4892922>
- [51] Markevich, A., Kurasch, S., Lehtinen, O., Reimer, O., Feng, X., Müllen, K., ... Besley, E. (2016). Electron beam controlled covalent attachment of small organic molecules to graphene. *Nanoscale*, *8*, 2711–2719. article. <https://doi.org/10.1039/C5NR07539D>
- [52] Melios, C., Panchal, V., Giusca, C. E., Strupinski, W., Silva, S. R. P., & Kazakova, O. (2015). Carrier type inversion in quasi-free standing graphene: studies of local electronic and structural properties. *Nature: Scientific Reports*, *5*, 10505. article. <https://doi.org/10.1038/srep10505>
- [53] Novikov, S., Lebedeva, N., Hämäläinen, J., Iisakka, I., Immonen, P., Manninen, A. J., & Satrapinski, A. (2016). Mini array of quantum Hall devices based on epitaxial graphene. *Journal of Applied Physics*, *119*(17), 174504. <https://doi.org/10.1063/1.4948675>
- [54] Novikov, S., Lebedeva, N., Manninen, A. J., & Satrapinski, A. (2016). Tests of Series Quantum Hall Arrays Based on Epitaxial Graphene. In *Digest on Conference on Precision Electromagnetic Measurements (CPEM2016)*. proceedings, IEEE. <https://doi.org/10.1109/CPEM.2016.7540653>
- [55] Satrapinski, A., Gotz, M., Pesel, E., Fletcher, N., Gournay, P., & Rolland, B. (2016). Testing the new generation of low-frequency current comparators. In *2016 Conference on Precision Electromagnetic Measurements (CPEM 2016)* (pp. 1–2). IEEE. <https://doi.org/10.1109/CPEM.2016.7540594>
- [56] Thodkar, K., Schönenberger, C., Calame, M., Lüönd, F., Overney, F., & Jeanneret, B. (2016). Characterisation of HMDS treated CVD Graphene. In *Digest on Conference on Precision Electromagnetic Measurements (CPEM2016)*. proceedings, IEEE. <https://doi.org/10.1109/CPEM.2016.7540498>